THEMIS characterization of the MER Gusev crater landing site

Keith A. Milam, Karen R. Stockstill, Jeffrey E. Moersch, Harry Y. McSween Jr., Livio L. Tornabene, and Amitabha Ghosh
Planetary Geosciences Institute, Department of Geological Sciences, University of Tennessee, Knoxville, Tennessee, USA

Michael B. Wyatt and Phillip R. Christensen
Department of Geological Sciences, Arizona State University, Tempe, Arizona, USA

Received 4 December 2002; revised 27 May 2003; accepted 3 June 2003; published 12 December 2003.

[1] Gusev crater, previously interpreted as the depocenter for the Gusev-Ma'adim Vallis fluvio-lacustrine system, is a proposed landing site for one of the Mars Exploration Rovers (MER). Here we use new remote-sensing data from the Thermal Emission Imaging System (THEMIS) supplemented by data from the Thermal Emission Spectrometer (TES), Mars Orbiter Camera (MOC), and Mars Orbiter Laser Altimeter (MOLA) to characterize the geology of Gusev crater. Thermal infrared data from THEMIS and TES were used to map thermophysical units on the basis of relative albedos and diurnal temperature variations. THEMIS and MOC visible images were used to map unit morphologies and to estimate crater density ages. MOLA data were used to identify unit contacts and stratigraphic relationships. Various data were then combined to construct a new surface unit map and stratigraphy for units on the floor of Gusev. Seven surface units were identified in Gusev, mostly Hesperian in age, but with two showing evidence of later modification and redistribution. Five or more surface units and layering are present within the MER-A landing ellipse, attesting to the geologic diversity of this site. Surface units show features that could be consistent with fluvio-lacustrine, aeolian, and/or volcanoclastic deposition, but the spatial resolution of visible/infrared data does not allow for the identification of unambiguous volcanic or fluvio-lacustrine textures. However, a MER landing in Gusev may provide the opportunity to analyze multiple units, distinguish rock types, examine stratigraphic relationships, and shed light on the ancient depositional environment. *INDEX TERMS:* 5464 Planetology: Solid Surface Planets: Remote sensing; 5470 Planetology: Solid Surface Planets: Surface materials and properties; 5494 Planetology: Solid Surface Planets: Instruments and techniques; 5415 Planetology: Solid Surface Planets: Erosion and weathering; 5460 Planetology: Solid Surface Planets: Physical properties of materials; *KEYWORDS:* THEMIS, Gusev crater, thermal infrared, MER, Mars Exploration Rover, landing site

Citation: Milam, K. A., K. R. Stockstill, J. E. Moersch, H. Y. McSween Jr., L. L. Tornabene, A. Ghosh, M. B. Wyatt, and P. R. Christensen, THEMIS characterization of the MER Gusev crater landing site, *J. Geophys. Res.*, *108*(E12), 8078, doi:10.1029/2002JE002023, 2003.

1. Introduction

[2] The focus of the Mars Exploration Program is the search for water, with the goal of identifying regions having the highest probability of capturing and preserving biomarkers. As a part of this program, two rovers are set to launch toward Mars in 2003 with early 2004 landings. Each Mars Exploration Rover (MER) will carry the Athena science package [see *Squyres et al.*, 2003] with instruments suitable for gathering evidence of ancient water on Mars. Each MER site has been evaluated for evidence of past water and the relatively low probability of hazards posed during landing. Prior to final landing site selection and mission operations, it is crucial that all available data sets from Mars orbiting spacecraft be analyzed to ascertain the potential scientific return of each site.

[3] Gusev crater is a ~160 km-diameter complex impact structure (Figure 1), centered at 14.64°S 175.36°E, within the Aeolis Quadrangle of Mars (USGS M 5M-15/202 RN, 1984). The location of Gusev at the terminus of the 900 km-long Ma'adim Vallis and geomorphic features within both landforms have led several researchers [*Schneeberger*, 1989; *Cabrol et al.*, 1993, 1998; *Grin et al.*, 1994; *Grin and Cabrol*, 1997a] to propose Gusev as a lacustrine depocenter for the Ma'adim Vallis drainage system. Interpretations by previous authors that are consistent with this hypothesis include: multiple terrace levels within Ma'adim Vallis [*Cabrol et al.*, 1994], evidence of stream migration [*Cabrol et al.*, 1997], debris lobes or "deltaic" deposits at the mouth of Ma'adim [*Schneeberger*, 1989; *Grin et al.,* 1997a; *Grin and Cabrol*, 1997b], and curvilinear ridges

0148-0227/03/2002JE002023$09.00

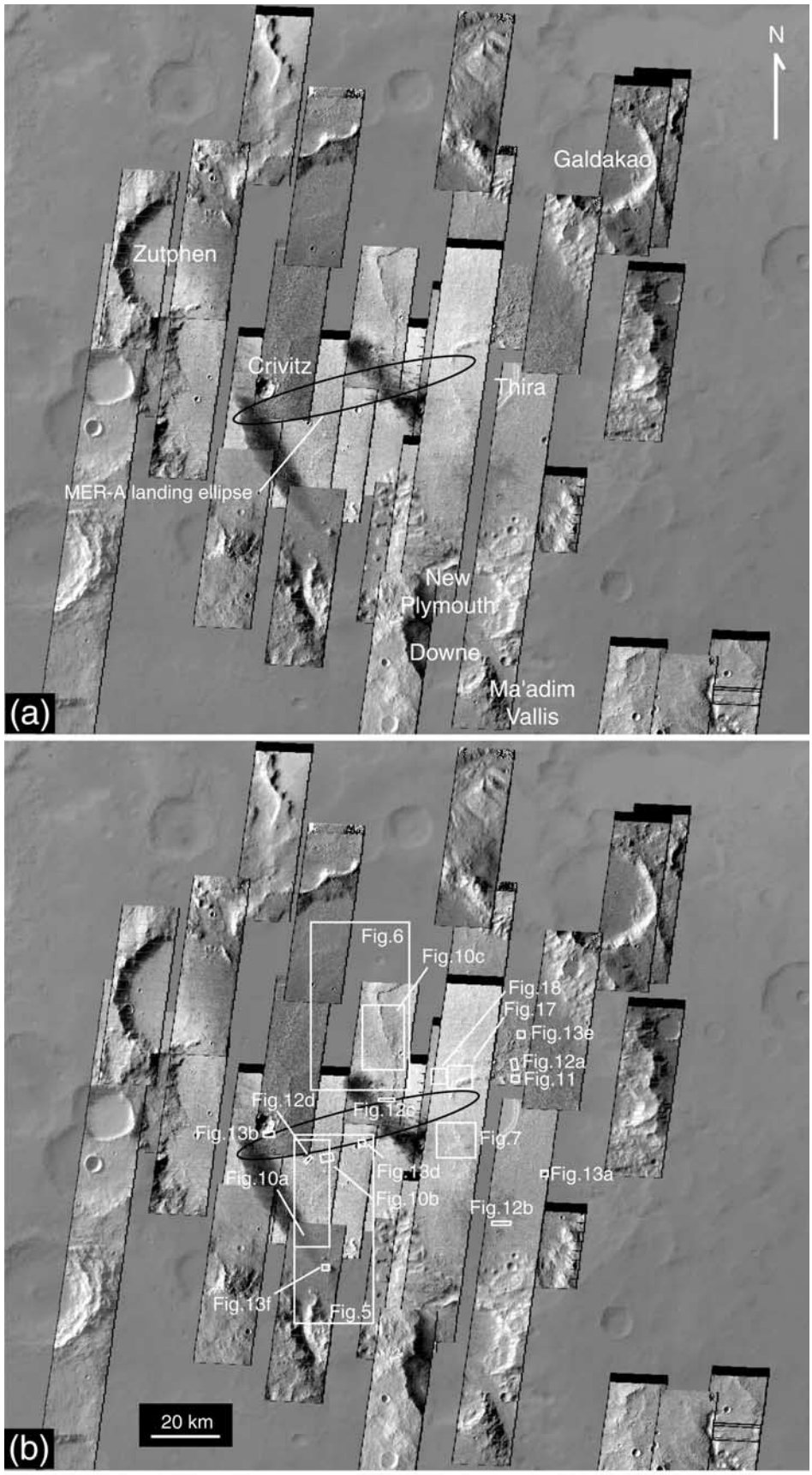

Figure 1. (a) Current THEMIS visible coverage overlain on MOC-MGS mosaic of Gusev crater. Black ellipse shown represents the MER-A landing ellipse (a 3-sigma probability of actual MER-A landing). (b) Reference map showing the locations of detailed figures described later.

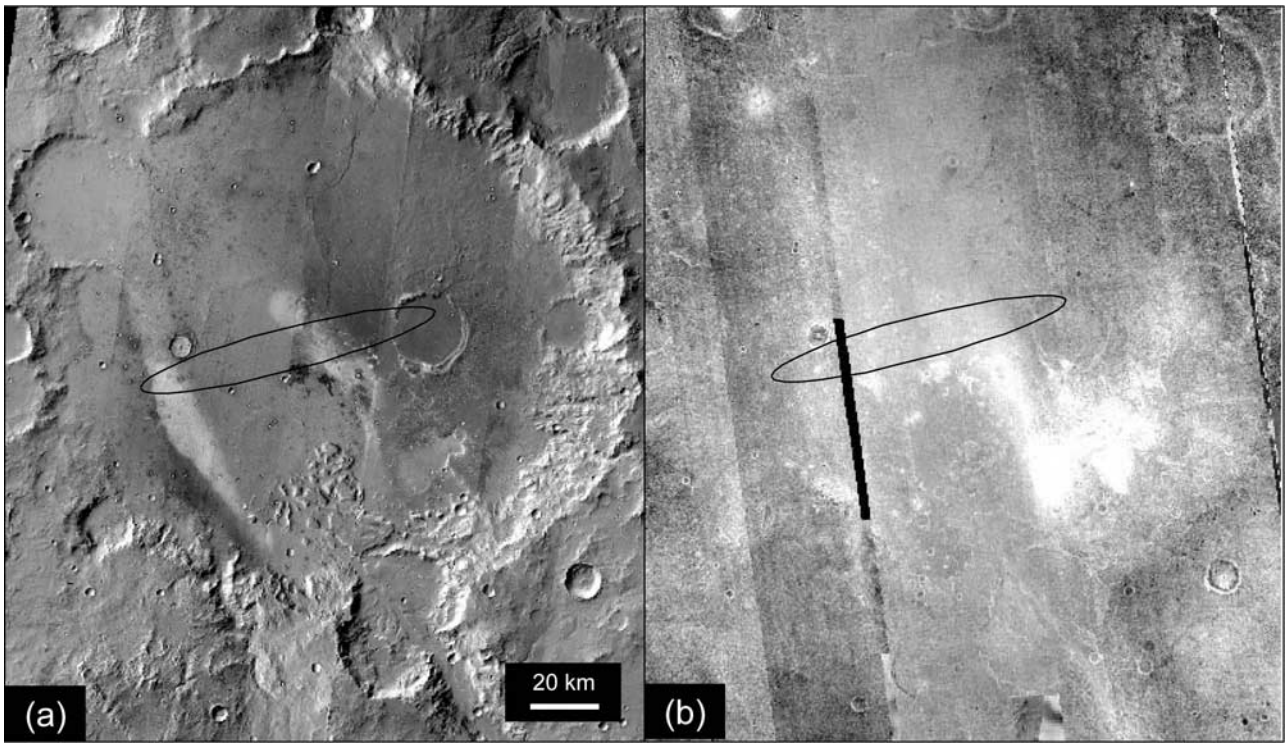

Figure 2. THEMIS (a) daytime TIR and (b) night TIR image mosaics (Band 9) for Gusev crater. Black ellipse shown represents the MER-A landing ellipse.

within Gusev analogous to sedimentary structures formed in terrestrial ice-covered lakes by sub-glacial rotary currents [*Grin and Cabrol.*, 1997a, 1997c]. Recent studies have also proposed this hydrologic system to have been active for 2 Ga over the Noachian-Hesperian periods [*Cabrol and Grin*, 1997; *Grin and Cabrol*, 1997b].

[4] Evidence of a paleolake in Gusev crater [*Masursky et al.*, 1988; *Landheim et al.*, 1993; *Cabrol et al.*, 1994; *Cabrol and Brack*, 1995; *Cabrol et al.*, 1996; *Cabrol and Grin*, 1997] makes it an attractive candidate for a MER landing [*Cabrol et al.*, 2002] for several reasons. First, potential lacustrine environments like Gusev may contain sedimentary structures (flow margins, shorelines, channels, ripple marks, etc.) or mineral deposits (evaporites, tufas, etc.) indicative of former aqueous activity [*Eugster and Hardie*, 1978]. Second, continuous settling of fine-grained sediment in terrestrial lacustrine environments leads to the burial and preservation of biomarkers. If life formerly existed on Mars, fluvio-lacustrine environments like Gusev would thus be a favored setting for fossil preservation [*Farmer and Des Marais*, 1999]. Also, relatively flat "lake beds" are devoid of many hazards posed to lander missions.

[5] Although there is much that may suggest an ancient lacustrine environment at Gusev, no unequivocal evidence (such as evaporite deposits or shorelines) has been found to confirm the proposed hypothesis. With this in mind, we take a first look at new data from the Mars Odyssey Thermal Emission Imaging System (THEMIS) to provide insight into the geologic environment of Gusev crater. This study also employs data from the Mars Global Surveyor (MGS) Thermal Emission Spectrometer (TES), Mars Orbiter Camera (MOC), and Mars Orbiter Laser Altimeter (MOLA) instruments to:

[6] • map surface units by their thermophysical and morphologic properties

[7] • derive a stratigraphic sequence

[8] • make comparisons with previous geologic surveys-with the ultimate aim of evaluating various depositional hypotheses for Gusev crater.

2. Methods

[9] Data from THEMIS, TES, MOC, and MOLA were used to provide thermophysical, morphologic, topographic, and temporal perspectives of Gusev crater. Thermal infrared (TIR) data from THEMIS and TES was first used to identify and map units on the basis of thermophysical properties (temperature and albedo). THEMIS visible and daytime TIR data, along with high-resolution MOC images, were then used to map units on the basis of morphology and texture. These data were also used for crater counting/age determination, and to search for evidence of layering. MOLA data provided elevations of contacts between units, estimations of strata thicknesses, and confirmation of unit boundaries.

[10] Data collected from THEMIS include visible images in 5 bands at 20 m/pixel spatial resolution and TIR images at 100 m/pixel spatial resolution using 8 spectral bands from 6.8 to 12.6 μm (1563–690 cm^{-1}). TIR images were collected during the Martian day ($\sim$1600 local solar time) and night ($\sim$0400 local solar time) to observe diurnal changes in surface temperatures [*Christensen et al.*, 2003]. THEMIS TIR bands were chosen for their usefulness in detecting relevant geologic materials including silicates, carbonates, and sulfates. Currently, THEMIS has collected 27 visible, 28 daytime, and 11 nighttime TIR images of Gusev, producing $\sim$75%, 100%, and 100% coverage for

each data set, respectively. Mosaics of each data type were produced for Gusev (Figures 1 and 2). Daytime and nighttime TIR images were used to compare and contrast the relative temperatures of surfaces within Gusev (by comparison of relative temperatures on gray scale normalized TIR images). *Relative* temperatures were qualitatively characterized as "hot", "warm", and "cold" on the basis of the relative pixel brightness in daytime and nighttime TIR images. Orbital variations result in the THEMIS instrument collecting images over a range of local solar times and seasons, producing temperature variations that are dependent on time-of-day and season. Normalizing images only allows for relative comparisons between individual THEMIS images within an image mosaic. For point of reference, within a single THEMIS night TIR image (I01511006 – Apr. 17, 2002, 23:14 local solar time), temperatures ranged from 174–196 K for units defined in this study. Daytime images showed comparable temperature contrasts. Visible and daytime TIR images were also used to measure crater densities for defined units (discussed later).

[11] TES [*Christensen et al.*, 1992, 2001] is a Fourier transform Michelson interferometer that collects TIR spectra over 1709–200 cm^{-1} (5.8–50 μm) with 5 and 10 cm^{-1} spectral sampling and 3 × 5 km spatial resolution. During its initial mapping phase, which lasted approximately 1 Martian year, TES collected approximately 5×10^7 spectra. Most of Gusev crater has been mapped by TES. TES spectra were used to note the presence of surface types 1 and 2 [*Bandfield et al.*, 2000] in Gusev, and a TES thermal inertia map by *Jakosky and Mellon* [2001] was used to determine thermal inertias of the more areally extensive units. TES bolometric data were used to measure relative albedo variations across surfaces. Albedos ranged from 0.19–0.26 and, when describing units, were categorized as "low" (<0.23) or "high" (≥0.23).

[12] Narrow-angle, high spatial resolution (1.46–5.68 m/pixel) MOC (Mars Global Surveyor) images were used to identify distinctive morphologies within Gusev. Surfaces that (a) were laterally extensive, (b) had consistent morphologic characters, and (c) occur within a specific range of elevations were identified as distinctive morphologic units. Viking Orbiter and THEMIS data were also used with MOC data to track larger-scale modifications to surfaces within Gusev. For more on the MOC instrument, see *Malin et al.* [1992] and *Malin and Edgett* [2001].

[13] MOLA is a laser altimeter used to collect high-precision elevation data from the Martian surface. MOLA fires 10 Hz (~8 ns) pulses toward the Martian surface and measures return times to calculate surface elevations with a vertical accuracy of <1 m [*Zuber et al.*, 1992; *Smith et al.*, 2001]. The MOLA team has produced global topographic grids for Mars at 1/128°, 1/64°, and 1/32° per pixel resolutions. Data from the 1/128° per pixel v. 2.0 MEGDR topographic grid (between 0°–44°S, 90°–180°E) were used to generate a topographic map for Gusev (Figure 3). This map, along with topographic profiles of key unit boundaries, was used to estimate the maximum and minimum elevations of floor units. Topographic relief was calculated as an indication of each unit's minimum thickness (assuming horizontality). Topographic profiles were used to identify prominent slope changes or "benches" that occur at constant elevations. Such identifiable slope breaks, where present, may represent contacts between units.

3. Identification of Units

3.1. Unit Nomenclature

[14] For this study, a primary objective has been to identify and delineate units on the floor of Gusev crater. Our approach has been to map units independently on the basis of their thermophysical and morphological properties and to highlight where correlations exist between the two techniques. When strong correlations between both types of units can be made, names have been shared. Unit names are denoted by two or three capital letters and, in most cases, have been derived from morphologic features of that particular unit. For clarity, subscripts "t" and "m" refer to the type of unit (thermophysical and morphological unit respectively). The combined results of thermophysical and morphologic unit mapping resulted in a surface unit map. To avoid developing an additional naming scheme for surface units, the original unit designations were maintained, but subscripts were dropped. Our naming system avoids using crater density ages as a part of unit designations because of the problems that surface modification by erosive/depositional processes presents to crater ages in the Aeolis quadrangle.

3.2. Thermophysical Properties

[15] Eight *thermophysical units* were identified in Gusev crater by qualitative comparisons of albedos and relative temperature differences (Table 1) derived from THEMIS and TES observations as described above. As used here, a thermophysical unit is defined as rock or sediment that is laterally extensive, defining an area with similar albedos and day/night relative temperature variations.

[16] The most obvious thermophysical unit is the Low Albedo (LA_t) unit (Figure 4a). As its name implies, LA_t has low albedos (Figure 1) and is hot in THEMIS daytime and nighttime TIR images (Figure 2). LA_t has a mean thermal inertia value of 240 ± 20 J m^{-2} K^{-1} $s^{-1/2}$, consistent with a surface whose average particle size is consistent with medium-grained sand [*Pelkey et al.*, 2001]. LA_t is presently split into two areas, a western area having sharp boundaries (as determined by visible and daytime TIR images) and an eastern area having more diffuse boundaries (visible and daytime/nighttime TIR). THEMIS nighttime TIR shows eastern LA_t extending farther southeast than is shown by daytime TIR imagery.

[17] A High Thermal Inertia (HTI_t) unit has been identified in southeastern Gusev using THEMIS and TES data (Figure 4a). Visibly, this unit has areas with both high and low albedos (Figure 1) and is warm to cold in daytime TIR (Figure 2a). Nighttime TIR shows this as a hot unit, occurring as eastern and western lobes (Figure 2b). Both lobes are centered around an irregular depression in southeastern Gusev. The eastern lobe appears as a THEMIS nighttime TIR hot unit with sharp, well-defined boundaries. Nighttime TIR images show that relative temperatures are more diffuse and boundary contacts less distinct for the western lobe. TES thermal inertia values for this area are ~400 ± 70 J m^{-2} K^{-1} $s^{-1/2}$. Such high thermal inertias are consistent with very coarse sand to granule particle sizes [*Pelkey et al.*, 2001].

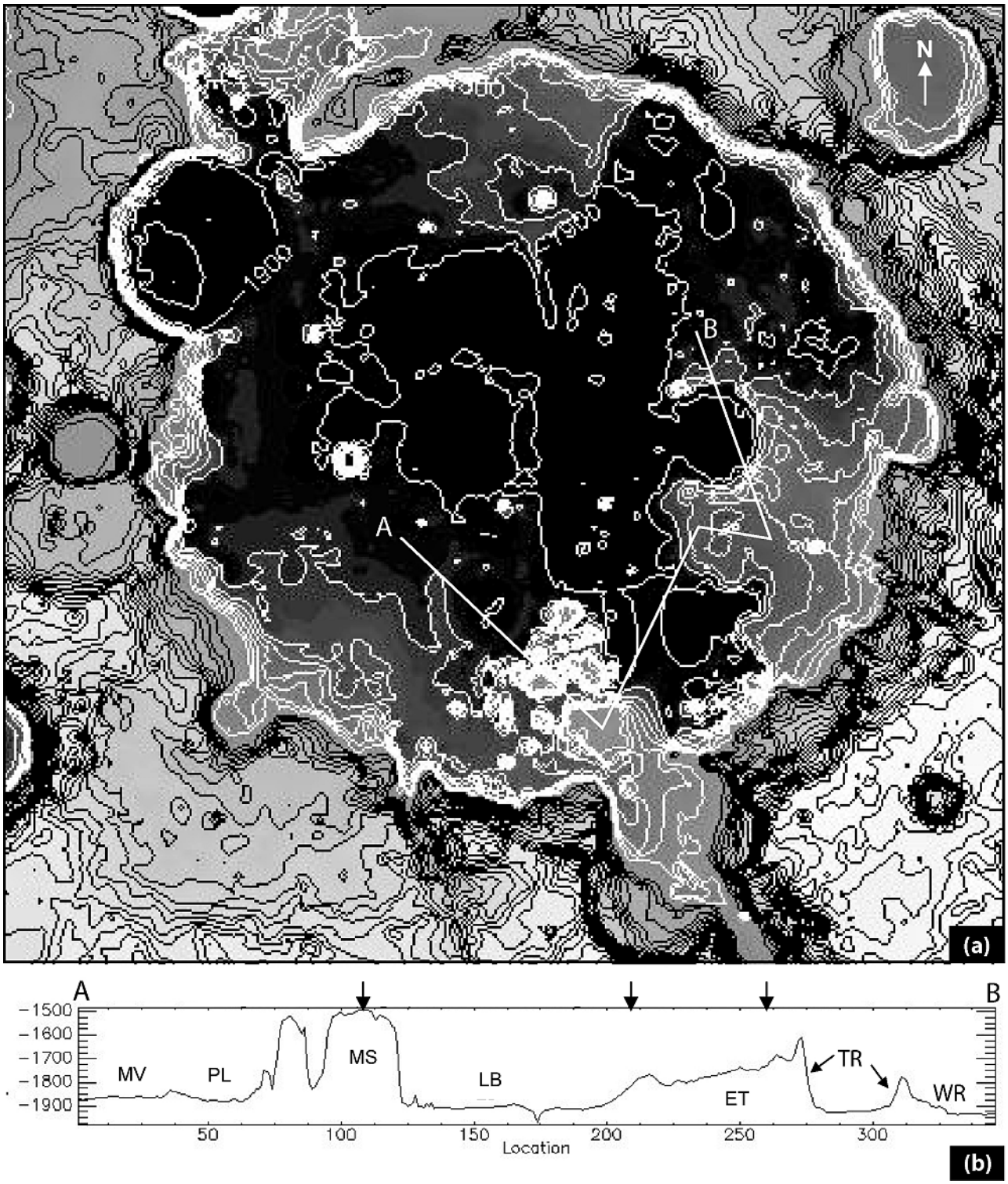

Figure 3. (a) Topographic map of Gusev crater generated from v.2.0 MEGDR MOLA global topographic grid. For clarity the contour interval (white contours) inside the crater (between −2200 and −1500 m below datum) is 50 meters; from the base of the rim outward (between −1500 and −2500 m), contour intervals of 100 m are used (black contours). (b) MOLA profile across most units within Gusev crater; profile line is shown in (a). Unit abbreviations are given in Table 1 and defined later. Arrows above profile indicate a change in profile orientation in (a).

Table 1. THEMIS Units Within Gusev Crater[a]

Units	Thermophysical Properties			Morphologic Properties	U.S.G.S. Equivalent Geologic Units[b]
	Vis.	Day IR	Night IR		
Ma'adim Vallis (MV)	high	warm	cold	- low ridges parallel to Ma'adim length (apparent flow direction) but do not extend into Gusev - smaller perpendicular ridges nearer to Gusev	$AHch_3$, $AHgf_2$
Plains (PL)	high	warm	warm craters (hot)	- smooth with moderately dense, small crater population	$AHgf_2$
Mesa (MS)	high	warm	tops: cold slopes: hot	- flat-topped surrounded by steep slopes	$AHbm_1$
Etched (ET)	high	cold	knobs: hot underlying: cold	- small knobs with rare "channelized" areas; devoid of most craters	$AHbm_1$, $AHgf_1$
Wrinkled (WR)	high	warm	warm craters: cold	- low subdued ridges trending NE-SW and N-S - older, degraded craters present	$AHbm_1$, $AHgf_1$
Thira Rim (TR)	high	warm	warm	- crater rim with collapsed terrace	c_2
Low Albedo (LA_t and low-albedo materials)	low	hot	hot	- overlapping wind streaks, tracks - multiple prevailing/local wind patterns - variable distributions with time	$AHgf_2$
High Thermal Inertia (HTI_t)	high/low	warm/cold	hot	- rough terrain with high thermal inertia (TES) and low-albedo deposits	$AHbm_1$, $AHgf_2$
Lobate (LB)	high	cold	warm/cold	- smooth unit with lobate terminal margins	$AHgf_1$

[a]The first six units occur as both thermophysical and morphological units, the second two units occur only as thermophysical units.
[b]*Kuzmin et al.* [2000].

[18] The Ma'adim Vallis (MV_t) unit extends from Ma'adim Vallis, through Downe and New Plymouth craters (Figure 1) onto the floor of Gusev crater (Figure 4a). THEMIS and MOC visible imagery do not indicate noticeable albedo variations between MV_t and adjacent units. Daytime TIR images show this unit as having warm temperatures, also making it indistinguishable from surrounding units. Nighttime TIR data does show this cold nighttime unit extending into Gusev toward a small unnamed crater (14.74°S, 174.82°E). Relative nighttime TIR temperatures show a discernible eastern boundary for the unit (Figure 5).

[19] The Plains (PL_t) unit extends from the terminus of Ma'adim to the northwest breach in the crater rim near Zutphen crater (Figure 4a). PL_t has a high albedo (Figure 1) with warm daytime and nighttime TIR temperatures (Figure 2). Thermal inertia values for PL_t are 290 ± 70 J m^{-2} K^{-1} $s^{-1/2}$, consistent with a surface dominated by coarse sand [*Pelkey et al.*, 2001]. Nighttime TIR images reveal that PL_t can be distinguished by the presence of craters with hot nighttime TIR rim material and ejecta (Figure 6). Daytime TIR images show PL_t as warm material with craters containing cooler ejecta (Figure 2a). These thermophysical characteristics are not common to other units within Gusev.

[20] The Mesa (MS_t) unit is present just north of the Ma'adim terminus (Figure 4a) and has been previously interpreted by others [*Landheim et al.*, 1994; *Grin and Cabrol*, 1997a, 1997b, 1997c] as deltaic sediment deposited by Ma'adim. The MS_t unit is composed of flat-topped positive relief features that are identifiable in visible images, have high albedos (Figure 1), and have warm temperatures in daytime TIR (Figure 2a). Mesas are separated by steep-walled valleys that are oriented in multiple directions. At night, MS_t mesas have relatively warm to cold tops and hot slopes (Figure 2b). Our observations are similar to those of other mesas on Mars [*Christensen et al.*, 2003]. A variety of scenarios could account for this temperature variation, such as well-indurated, coarse-grained rock overlain by unconsolidated sediment cover, changes in grain size or porosity, or the contribution of nighttime radiative heating from nearby lowlands reflected off MS_t slopes, thus contributing to their increased temperatures at night. MS_t can be distinguished from PL_t by the lack of craters with hot nighttime TIR rim material that are common to PL_t.

[21] The Etched (ET_t) unit occurs in the southeastern quadrant (Figure 4a) beyond the rim of Thira crater (14.46°S, 175.75°E). ET_t has a high albedo, is relatively cold in daytime TIR, and in nighttime TIR has a "mottled" (warm-cold) appearance (Figures 1 and 2). ET_t's "mottled" nighttime TIR temperature correlates with its dissected nature. ET_t's landscape represents an erosional surface (warm nighttime TIR areas) superimposed upon distinctive underlying material (cold nighttime TIR areas). The northern and southwestern thermophysical boundaries of ET are gradational with adjacent units.

[22] The Wrinkled (WR_t) unit occupies the northeastern quadrant of Gusev and the central region of the crater (Figure 4a). WR_t has a high albedo and warm daytime and nighttime TIR temperatures (Figures 1 and 2), with a thermal inertia of 200 ± 20 J m^{-2} K^{-1} $s^{-1/2}$, consistent with

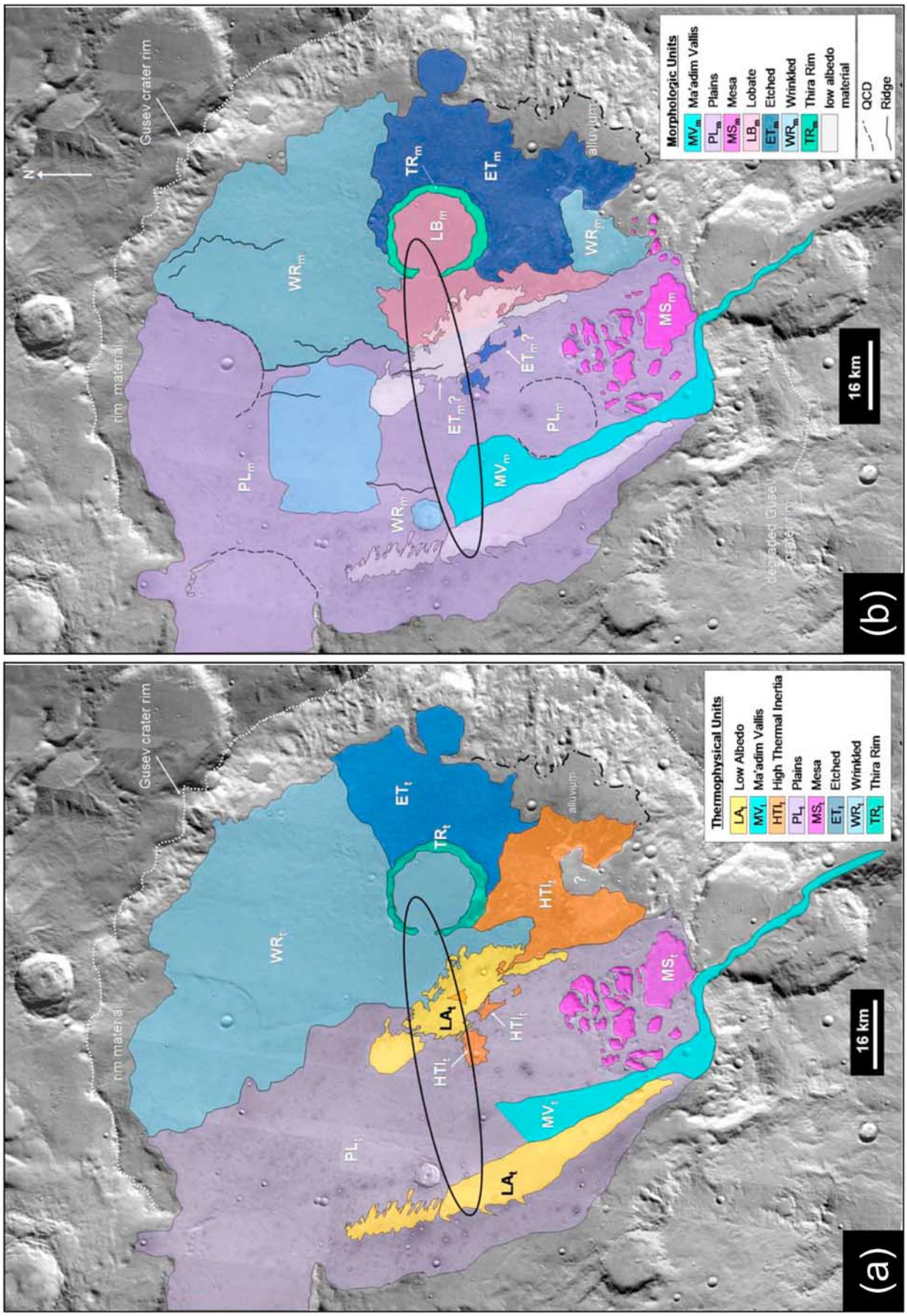

Figure 4. Maps of (a) thermophysical units and (b) morphologic units Gusev crater (overlain on THEMIS day IR image mosaic). Black ellipse represents MER-A landing ellipse.

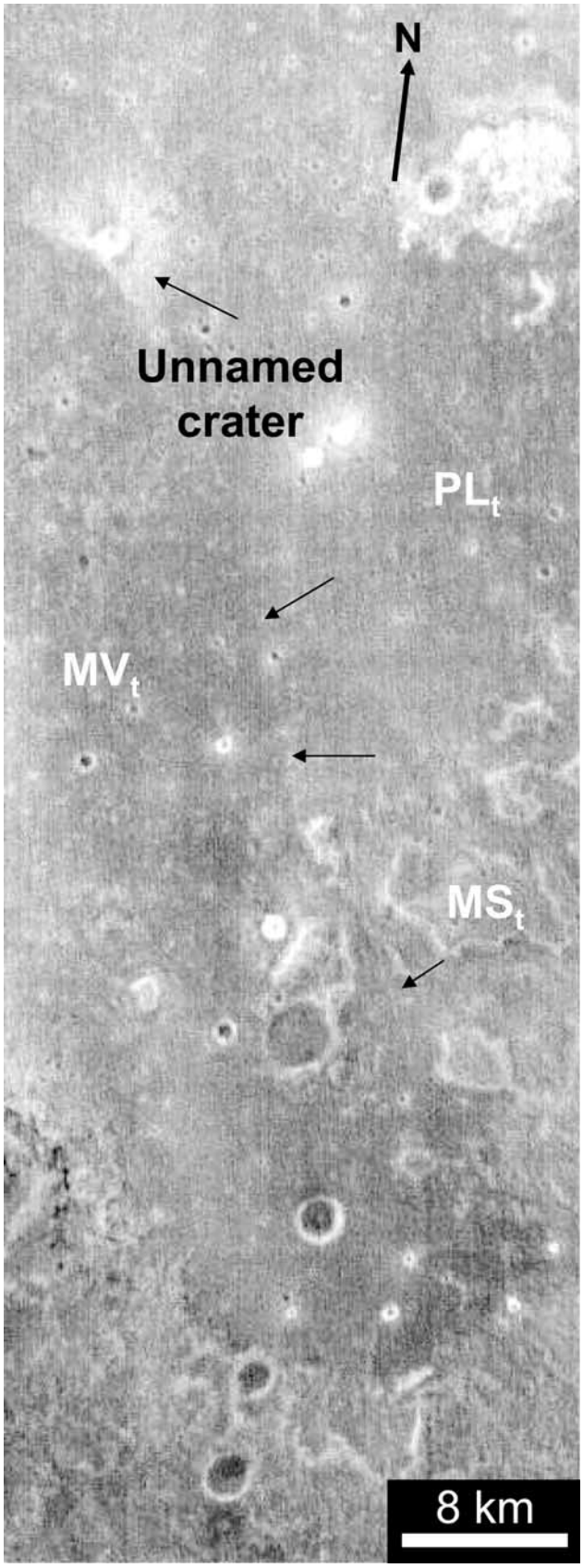

Figure 5. THEMIS night IR image (I01873002) showing eastern boundary (arrows) of Ma'adim Vallis thermophysical (MV_t) in Gusev crater. "Forbidden zone" of missing crater ejecta can be seen to the southwest of unnamed crater.

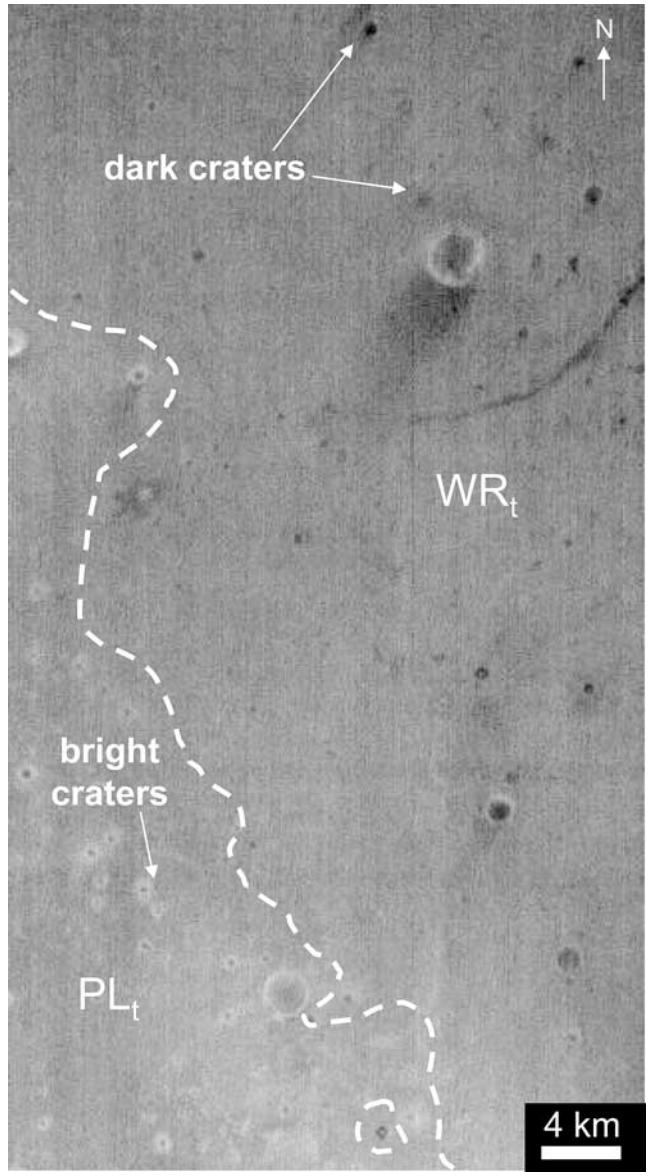

Figure 6. THEMIS night IR image (I01511006) showing dark craters distinctive of WR_t and bright-rimmed craters of PL_t.

a surface covered mostly in fine-grained sand [*Pelkey et al.*, 2001]. A distinguishing thermophysical property of WR_t is the abundance of small (typically <2 km diameter) craters whose floors are cold in nighttime TIR (Figure 6).

[23] The Thira Rim unit (TR_t,), located just to the northeast of Gusev's center (Figure 4a), is comprised of rim material from this crater (~20 km diameter; 14.45°S 175.75°S) and associated collapsed terrace blocks. Most non-sloping TR_t material has a high albedo and is intermediate in daytime and nighttime TIR images (Figures 1 and 2); however, sections containing low-albedo material that are very hot in nighttime TIR images exist along the southern part of the rim (Figure 7). It is unclear whether these low-albedo areas are deposits along the rim, represent actual exposures of bedrock along Thira crater, and/or are wind-blown LA_t. On the basis of our method of defining thermophysical units, for now we tentatively consider the low-albedo areas as LA_t.

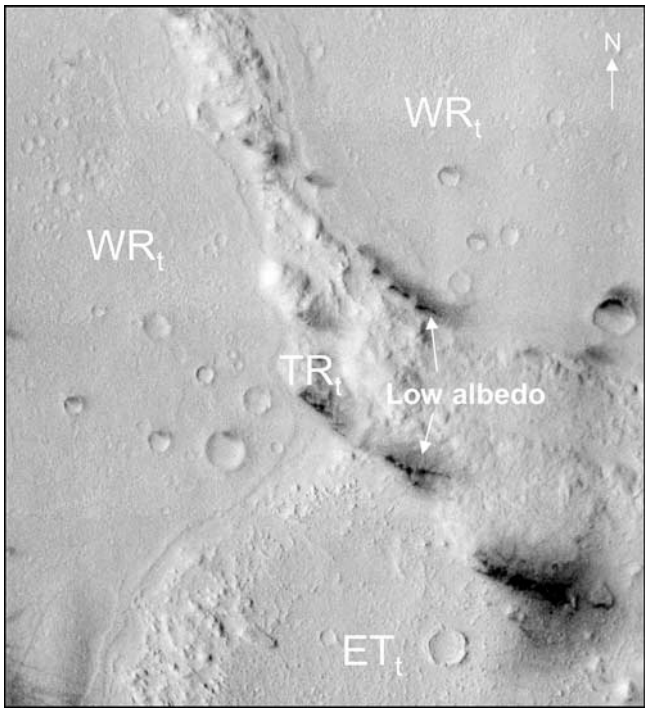

Figure 7. THEMIS visible image (V01580003) showing TR_t, associated low-albedo areas, and the contact between TR_t, WR_t, and ET_t units.

Thermophysical properties of TR_t are comparable to the PL_t, ET_t, and WR_t units, however, TR_t can still be distinguished from these units. TR_t lacks cold and warm craters present in WR_t and ET_t respectively. It also lacks the mottled surface common to ET_t.

3.3. Morphological Characteristics

3.3.1. Unit Descriptions

[24] An independent assessment of THEMIS and MOC visible images was used to identify *morphologic units* on the basis of distinguishing morphologic characteristics (Table 1). As applied here, a morphologic unit is defined as a laterally extensive unit with a homogeneous surface texture that occurs within a specific range of elevations. Seven distinct morphologic units were identified (Figure 4b), many corresponding to previously identified thermophysical units (Figure 4a).

[25] MV_m (Figure 8a) can be identified in Ma'adim Vallis on the basis of the presence of subdued ridges parallel to longitudinal axis of the valley. This morphological expression, however, does not appear to extend into Gusev Crater. In fact, the area within Gusev that was previously defined (thermophysically) as MV_t has surface textures very similar to PL_m. Despite this, an escarpment, corresponding to the suggested thermophysical boundary for MV_t extends from Ma'adim into Gusev and to the east of a small crater (Figure 9a). This suggests that MV_m may extend into Gusev as a localized unit.

[26] PL_m (Figure 8b) is relatively flat (with a slight north-south slope) and has a lower crater density than MV_m. Most of the larger craters in PL_m appear degraded, although there is a population of small (<1 km diameter) craters with well-defined rims. West-northwest to east-southeast linear dust-devil tracks (Figure 9b), similar to those identified elsewhere in MOC data by *Malin and Edgett* [2001], are superimposed on PL_m, showing the effects of wind activity on this unit. PL_m lacks exposure in eastern Gusev and appears to terminate in the east along a steep escarpment (Figure 9c).

[27] MS_m occurs as flat-topped mesas, flanked by slope debris, with a population of small (<1 km diameter) craters superimposed on mesa-tops (Figure 8c). Exposures of this unit are separated by narrow canyons, which suggest this unit was once continuous and subsequently eroded.

[28] A morphologic unit not distinguishable by its thermophysical properties is the Lobate Unit, LB_m (Figure 8d). LB_m occurs to the east of PL_m in central Gusev and has thermophysical properties similar to WR_t. LB_m can be distinguished by its lobate margins along its eastern boundary (Figure 8d). LB_m extends from the PL_m unit boundary, is deposited against ET_m south of and within Thira crater, and overlies WR_m in central Gusev.

[29] The distinctive morphologic characteristic of ET_m is a series of low knobs, small mesas, and interspersed dunes superimposed upon a relatively flat underlying surface, giving it an ''etched'' appearance (Figure 8e). Most of the knobs appear to be randomly oriented, whereas some in the southernmost part of this unit show a weak northwest-southeast orientation. In the northwestern parts of ET_m, channel-like features are present, suggesting some fluid modification (Figure 10).

[30] WR_m (Figure 8f) consists of subdued, northeast-southwest and north-south oriented ridges (producing a ''wrinkled'' appearance) with superimposed craters having degraded rims and infilled floors. The distinctive WR_m morphology is found in northeast and central Gusev and along the floor of the depression in southeast Gusev mentioned earlier. Some of the ridges appear to form longer ''fronts'' that have been interpreted by *Grin and Cabrol* [1997c] as evidence for rotary currents under a glacier-covered Gusev paleolake. However, ridge orientations are mostly north-south, showing no evidence of changing ''rotary'' orientations around Gusev.

[31] The TR_m unit (Figure 8g) is exposed crater rim material from Thira crater, with ET_m, LB_m, and WR_m deposited against it. The degraded rim of TR_m lacks a sizable crater population and has inward margins showing several slope breaks (variable elevation) around ~80% of the crater. Observations of the lack of ejecta superimposed upon adjacent units and termination of lateral deposition against TR_m also suggest that the Thira impact was one of the earliest events in Gusev and sampled distinctive strata from depth.

[32] Examination of the area previously identified as HTI_t reveals that, morphologically, the eastern lobe coincides with and shares the same morphology as ET_m. The western lobe shares the same surface textures as PL_m, LB_m, and WR_m, while the depression between the two lobes resembles WR_m with a thin mantling of low-albedo material. Because surface textures for HTI_t vary greatly across this area, it is not a true morphologic unit but an area of PL_m, WR_m, ET_m, and LB_m that share similar nighttime TIR temperatures. A thin mantling of low-albedo material or the mantling in combination with the rough landscape of this area in this region may be responsible for its nighttime TIR signature.

[33] Additional scrutiny of THEMIS and MOC visible imagery (Figure 8h) of the low-albedo areas (defined as the

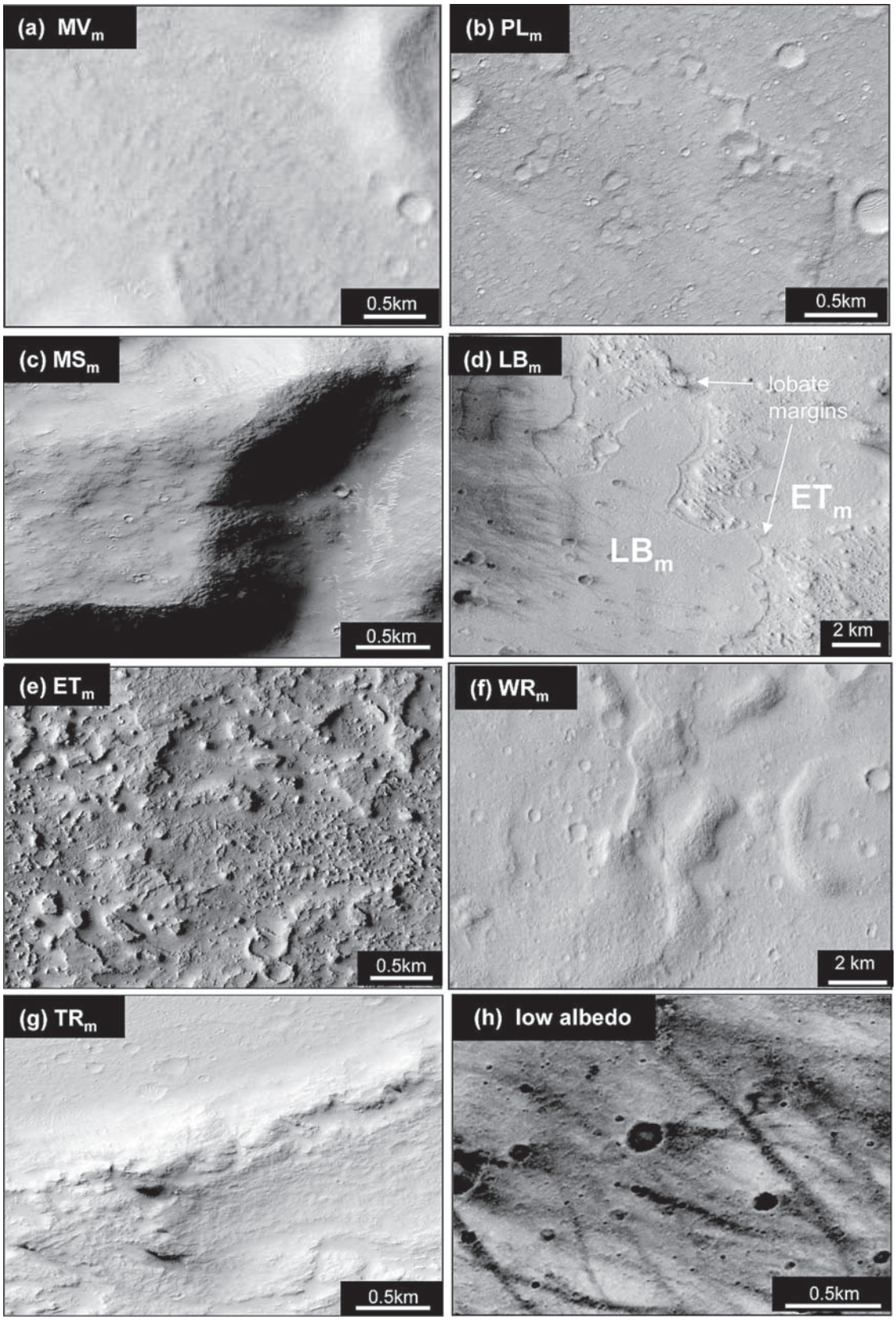

Figure 8. Characteristic textures of Gusev morphologic units and low-albedo materials. Units are as follows: (a) MV_m-Ma'adim Vallis (THEMIS-V02304003), (b) PL_m-Plains (THEMIS-V01243002), (c) MS_m-Mesa (MOC-E0300012), (d) LB_m-Lobed (THEMIS-V01580003) (e) ET_m-Etched Terrain (MOC-E0501350), (f) WR_m-Wrinkled (THEMIS-V02060002), and (g) TR_m-Thira Rim (MOC-E0201453). Also shown (f) is low-albedo material (THEMIS-V00881003).

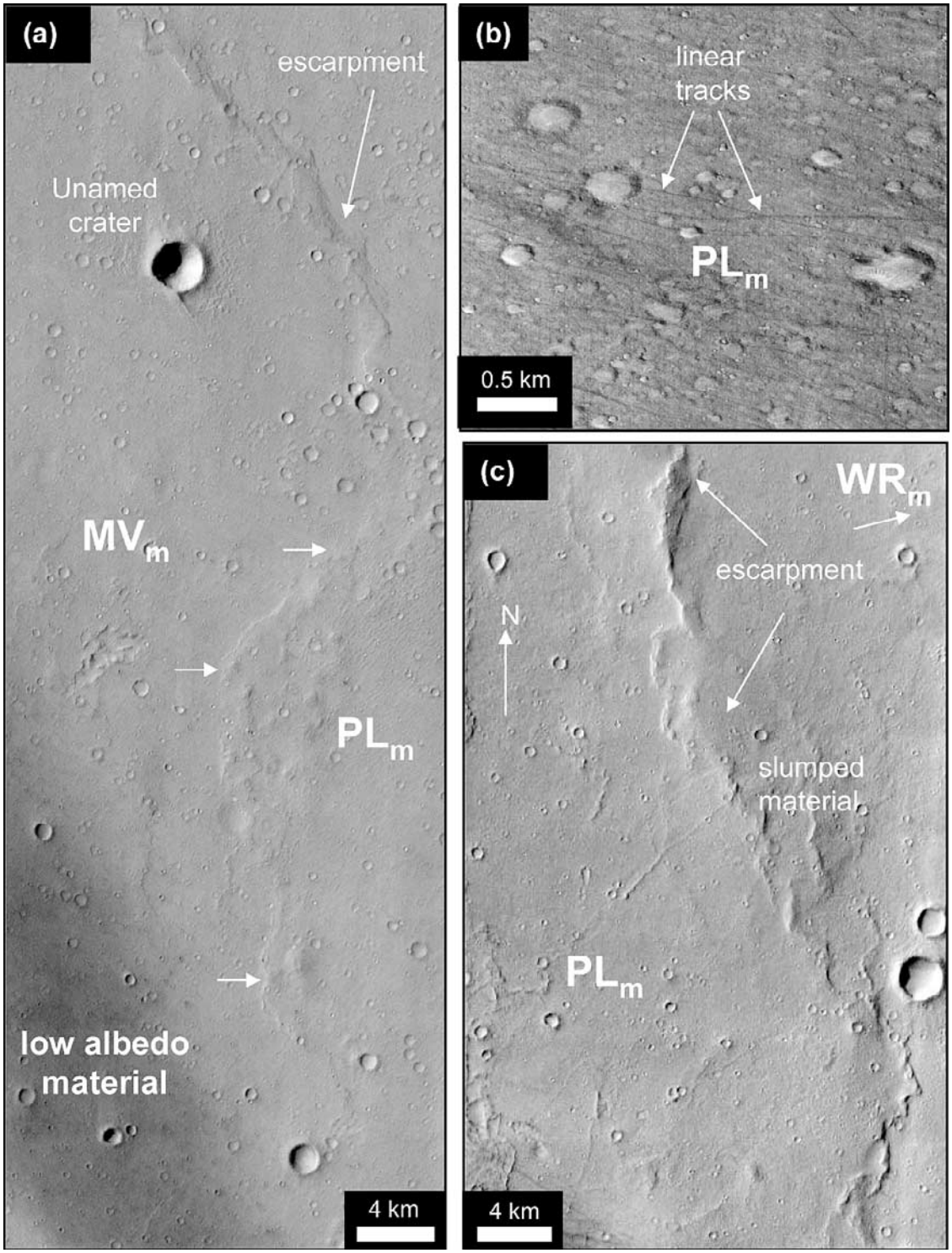

Figure 9. Selected features of morphologic units within Gusev: (a) MV_m unit boundary (arrows) (THEMIS-V02691003), (b) linear tracks superimposed on PL_m (MOC -E1103034-03), and (c) eastern boundary of PL_m (THEMIS-V03415003).

LA_t thermophysical unit) shows what appears to be the agglomeration of northwest-southeast oriented dust devil tracks, wind streaks, intracrater deposits, and possible blanketing material. Within the northwest-southeast prevailing wind pattern, track and streak orientations vary from due east to 50°SE, suggesting localized variations in wind direction. The western low-albedo area occurs as a continuous exposure of material grading northward into agglomerated northwest-southeast dust-devil tracks/wind streaks. The low-albedo material is somewhat ephemeral, having been observed to change position and orientations over the past 25 years (Figure 11). Low-albedo patterns are spatially associated with and trending toward the southern and northwest breaks in Gusev's crater rim (possible source

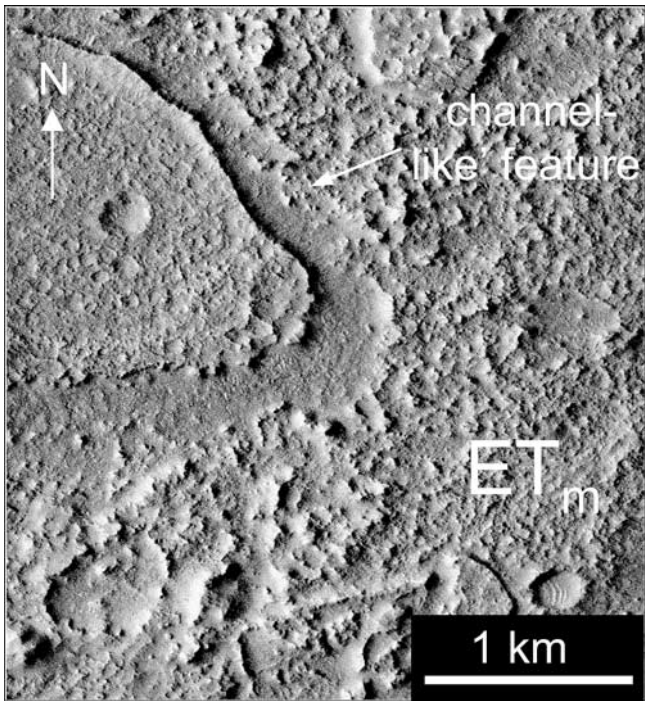

Figure 10. "Channelized" areas in northern ET_m (MOC-E051350).

areas for wind). This, coupled with the dust devil/wind streak phenomenon, suggests that this material is associated with the aeolian processes of scouring and/or deposition. It is unclear whether deposition, erosion, or both are being represented. Although the low-albedo material does appear to correspond with morphologic features in Gusev, we do not consider it a *morphologic* unit as defined in this paper. While laterally extensive in some parts of Gusev, this unit does occur at a variety of elevations corresponding to the PL_m, WR_m, LB_m, and possibly TR_m units. This suggests that either these units are being blanketed by material or are being eroded to reveal underlying lower albedo material. Thus low-albedo materials represent the effects of aeolian activity rather than a coherent unit.

3.3.2. Morphologic Unit Contacts

[34] Morphologic unit contacts in Gusev were delineated by differences in morphology and were often found to correspond with marked changes in elevation (Figure 3b). The boundary between the ET_m and WR_m in northeastern Gusev corresponds to a gradual change in slope and morphology, grading from ET_m to WR_m northward (Figure 12a). In southeastern Gusev, however, the boundary between ET_m and WR_m is marked by a steep escarpment and a pronounced change in morphology (Figure 12b). At the westernmost extent of ET_m, to the southwest of Thira crater, lobe margins for LB_m terminate at ET_m (Figure 8d).

[35] The exact eastern boundaries of the PL_m unit are less distinguishable visibly because of the presence of low-albedo material. However, the boundary is defined by a noticeable slope break (~ -1880 m to -1939 m) along an east-west transect (Figure 12c). Unit boundaries for TR_m and MS_m are also distinguished by their respective morphologies and topographic relief along unit boundaries; however, some contacts are more difficult to define.

[36] Nighttime TIR data gives the appearance that MV_t truncates a small unnamed crater's ejecta (Figure 5). Analysis of crater ejecta patterns, however, reveals that this crater was likely formed by an oblique impact from the southwest. This style of impact resulted in a "forbidden zone" of ejecta on the uprange side of the crater rim (Figures 12d and 5), which is typical of oblique impacts [*Pierazzo and Melosh*, 2000]. MOLA profiles show an asymmetric profile to the crater, further indicating an oblique impact (Figure 12d). This suggests that the northernmost boundary for MV_t does not actually truncate the crater ejecta. Linear margins, one of which corresponds to MV_t eastern boundary, do suggest that MV_m does extend onto the floor of Gusev north of the crater (Figure 9a).

3.3.3. Layering Within Morphologic Units

[37] Of the 7 identified morphologic units within Gusev, four show evidence of layering. Most layers are exposed at constant elevations, possibly indicating horizontal to subhorizontal strata, and each appears to be of uniform thickness. Because exposures are not abundant in Gusev, most layering is observed along the steep slopes of crater walls and escarpments (Figure 13). An unnamed,

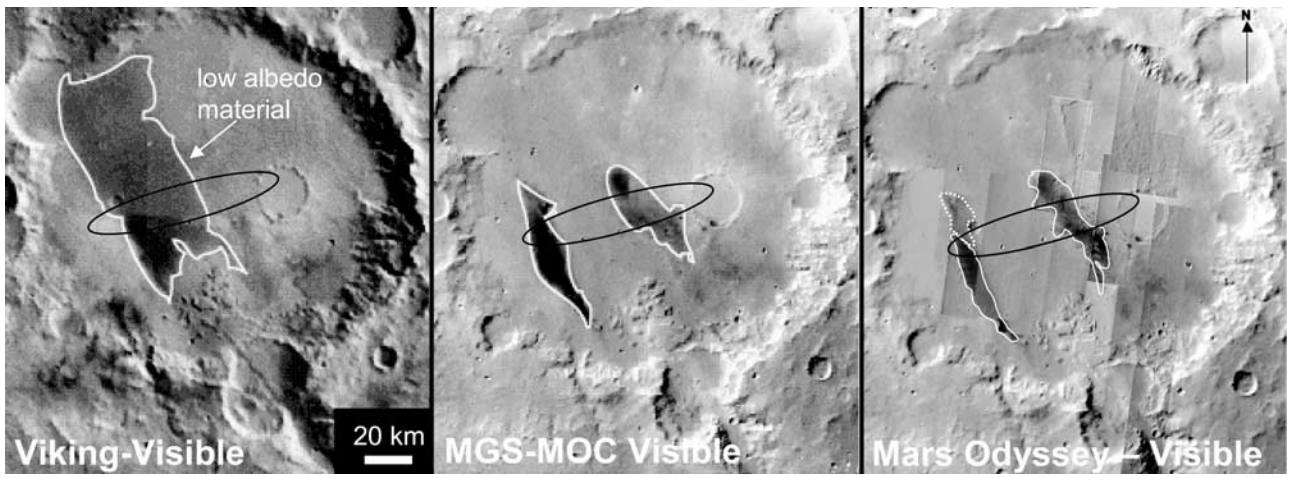

Figure 11. Viking Orbiter, MGS-MOC, and Mars Odyssey-THEMIS visible image mosaics of Gusev showing the redistribution of low-albedo materials during the past 25 years.

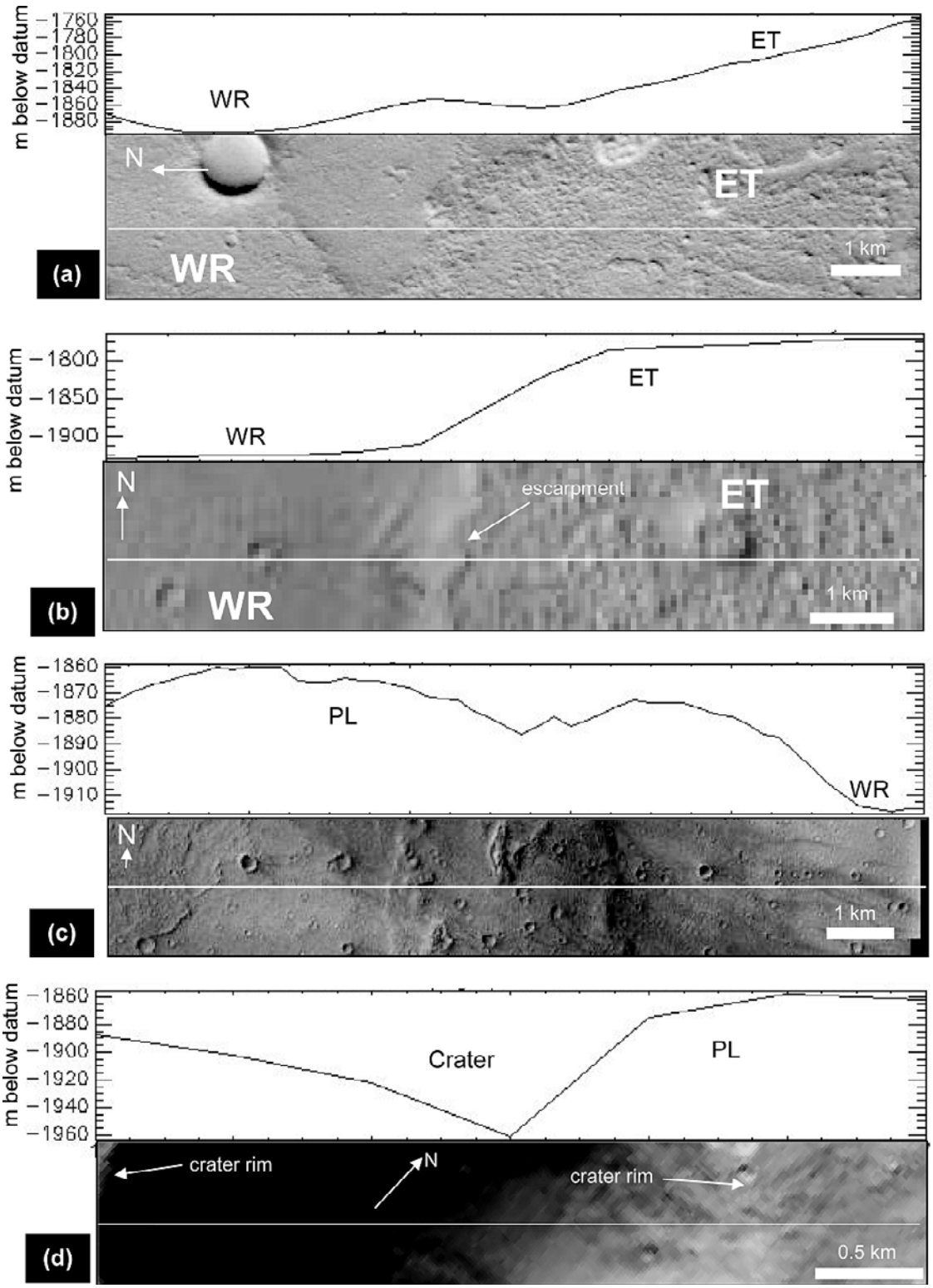

Figure 12. MOLA profiles of select features in Gusev crater: (a) North-south topographic profile across the WR_m-ET_m unit boundary in northeastern Gusev with THEMIS visible image (VO2666002) showing the gradual change from ET_m (in the south) to WR_m (in the north). (b) East-west topographic profile across the WR_m-ET_m boundary in southeastern Gusev; profile shown on THEMIS visible image (V03028003) showing the unit boundaries between WR_m and ET_m. (c) Topographic profile across the contact between PL_m and WR_m (THEMIS-V03415003). (d) Topographic profile across unnamed crater (THEMIS-V02691003).

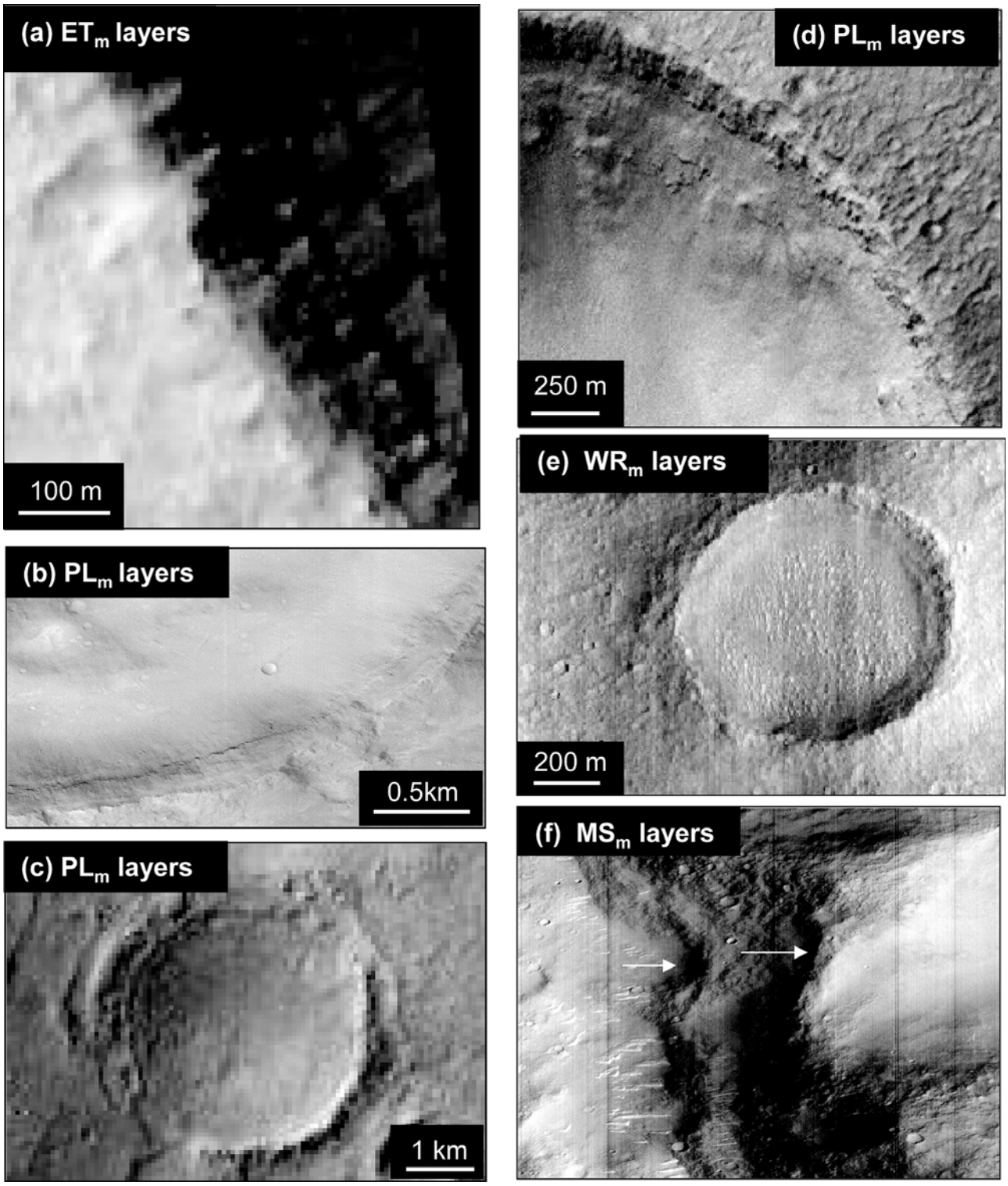

Figure 13. Evidence of layering within Gusev crater in (a) ET_m (MOC-M0202129), (b-d) PL_m (MOC-E1002768, E0503287, E1700827), (e) WR_m (THEMIS-V02666002), and (f) MS_m units (MOC-M0306211).

3.8 km-diameter impact crater within the ET_m in southeastern Gusev (14.83°S, 176.08°E), exposes several layers within its wall (Figure 13a). Some layers form cliffs while others form shallow slopes. Elevations of exposed layering in the western crater wall are between −1671 and −1789 m below datum, coinciding with ET_m elevations. This indicates that the uppermost ET_m is composed of several layers. Layers appear to be approximately horizontal, corresponding to given elevations along the crater wall.

[38] Three craters expose layering within the PL_m unit. The first crater (Figure 13b), 6.5 km in diameter (14.54°S,

174.57°E), shows layers exposed along its southeastern wall between −1899 and −1939 m (corresponding to PL_m elevations). A second crater (Figure 13c), at 14.32°S 175.13°E, shows layers exposed along the entire crater wall at elevations between −1884 and −1898 m. The third crater (Figure 13d) at 14.68°S 175.07°E shows several layers exposed approximately between −1843 and −1926 m.

[39] At least four craters in northeastern Gusev expose layering within the WR_m unit to the northeast of Thira crater. An example is a <0.8 km diameter crater (14.04°S 176.08°E), exposing several layers between −1850 and −1900 m within its crater wall (Figure 13e). Layers are highlighted by shadowing and, in this case, slight albedo differences. Weathering profiles are also accentuated by shadowing effects.

[40] MS_m shows some evidence of indistinct, subhorizontal layering. One mesa (15.23°S, 175.04°E) shows layers between −1800 and −1875 m, along eastward-facing exposures (Figure 13f).

4. Discussion

4.1. Proposed Surface Units

[41] Comparison of thermophysical and morphologic unit properties shows a strong spatial correlation between many of the two unit types. This supports our approach of using these properties independently to identify prominent surface units. However, it is important to note that the thermophysical properties of a given unit can vary laterally depending on a variety of factors such as grain size, facies changes, extent of cementation, degree of erosion/weathering, etc. Also, TIR data from the Martian surface is only representative of the top few centimeters of exposed material. If units are mantled by aeolian dust, thermophysical mapping can be problematic. Thus, when observing discrepancies between thermophysical and morphologic units and trying to determine true unit boundaries, morphologic delineation is, at the moment, preferred. In many cases, sudden slope changes correspond more closely with morphologic changes rather than thermophysical ones, further supporting use of morphology as the deciding factor for delineating unit boundaries.

[42] Recognizing the correlations between thermophysical and morphologic units, we propose seven *surface units* within Gusev crater. Here we use the term surface unit to define rock or sediment that (1) are laterally extensive or mappable, (2) express similar surface morphologies, (3) possess similar thermophysical qualities, and (4) occur over consistent elevation ranges across the mapped area. Surface unit abbreviations are indicated by the absence of a subscript. A surface unit map for Gusev crater is shown in Figure 14a. The proposed surface units are Thira Rim (TR), Wrinkled (WR), Etched (ET), Lobate (LB), Plains (PL), Mesa (MS), and Ma'adim Vallis (MV).

4.2. Surface Unit Elevations and Thicknesses

[43] MOLA data (Figure 3) provide a means of measuring the maximum and minimum elevations of exposed units within Gusev. Elevation data allows comparison the relative vertical positions of different surface units (Figure 15). For example, Figure 15 shows that the highest exposed surface unit within Gusev is MS, while the lowest exposed units are WR and LB. Topographic relief (calculated from maximum and minimum unit elevations) was assumed to represent minimum unit thicknesses (Figure 15). Marked slope breaks at constant elevations also provided a means of further delineating suspected unit boundaries and identifying exposures of underlying units (Figure 3b).

4.3. Crater Densities

[44] In an effort to determine relative and absolute ages of identified units, crater density measurements were made according to methods of the *Crater Analysis Technique Working Group* [1979]. Results of crater counts, measurements of surface areas, populations of craters ≥1, 2, 5, and 16 km, and age estimates are reported in Table 2 and summarized in Figure 16. Crater density measurements identify many of the units as Late Noachian to Late Hesperian in age, with WR Early Amazonian in age. Because no craters or ejecta are superimposed on low-albedo material and due to their very recent (<25 yrs.) redistribution within Gusev, this material is obviously Late Amazonian in age. Ages are mostly consistent with age estimates by *Kuzmin et al.* [2000].

4.4. Surface Unit Stratigraphy

[45] The combination of surface unit mapping (Figure 14a), elevation data (Figure 15), and crater density ages (Figure 16) provides a means of determining the stratigraphy (Figure 14a) and thus the depositional/erosional history of Gusev crater. Ages based on crater densities for Gusev units should be considered with caution. Planetary surfaces that undergo modification by processes other than impact cratering can give problematic crater ages [*Edgett and Malin*, 2003]. Factors such as erosion by wind or water, infilling, and the duration of exposure can lead to the obliteration of craters and therefore influence age estimates for such surfaces. With the presence of drainage and aeolian features within the Aeolis Quadrangle, age dating surface units is problematic and should only be considered within the context of topographic and other data.

[46] The lowest (elevation) stratigraphic units within Gusev appear to be TR and WR. Exposed TR lies between −1625 and −1900 m and WR is exposed between −1875 and −1975 m. From these elevations, it appears that WR lies below TR. However, WR is deposited against Thira's rim to the north (Figure 17). This indicates that TR existed prior to WR deposition, making TR the oldest unit within Gusev. The absence of superimposed craters (and thus lack of a crater density age) on TR is likely related to prolonged rim modification. The high elevation of TR likely led to an increased likelihood of modification by surficial and atmospheric processes. Also, several collapsed terrace blocks lie along the rim, indicating that Thira has been modified by crater wall collapse.

[47] Both WR and LB lie at comparable elevations, but LB appears to have an older crater density age. A comparison of the state of crater rims within both units (Figure 8) shows WR rims to be more degraded than those of LB, suggesting that WR is actually older than LB. If WR craters had been modified or even obliterated over time, crater density ages would represent the period during which modification took place, rather than deposition of WR. Additional support for an older WR comes from north

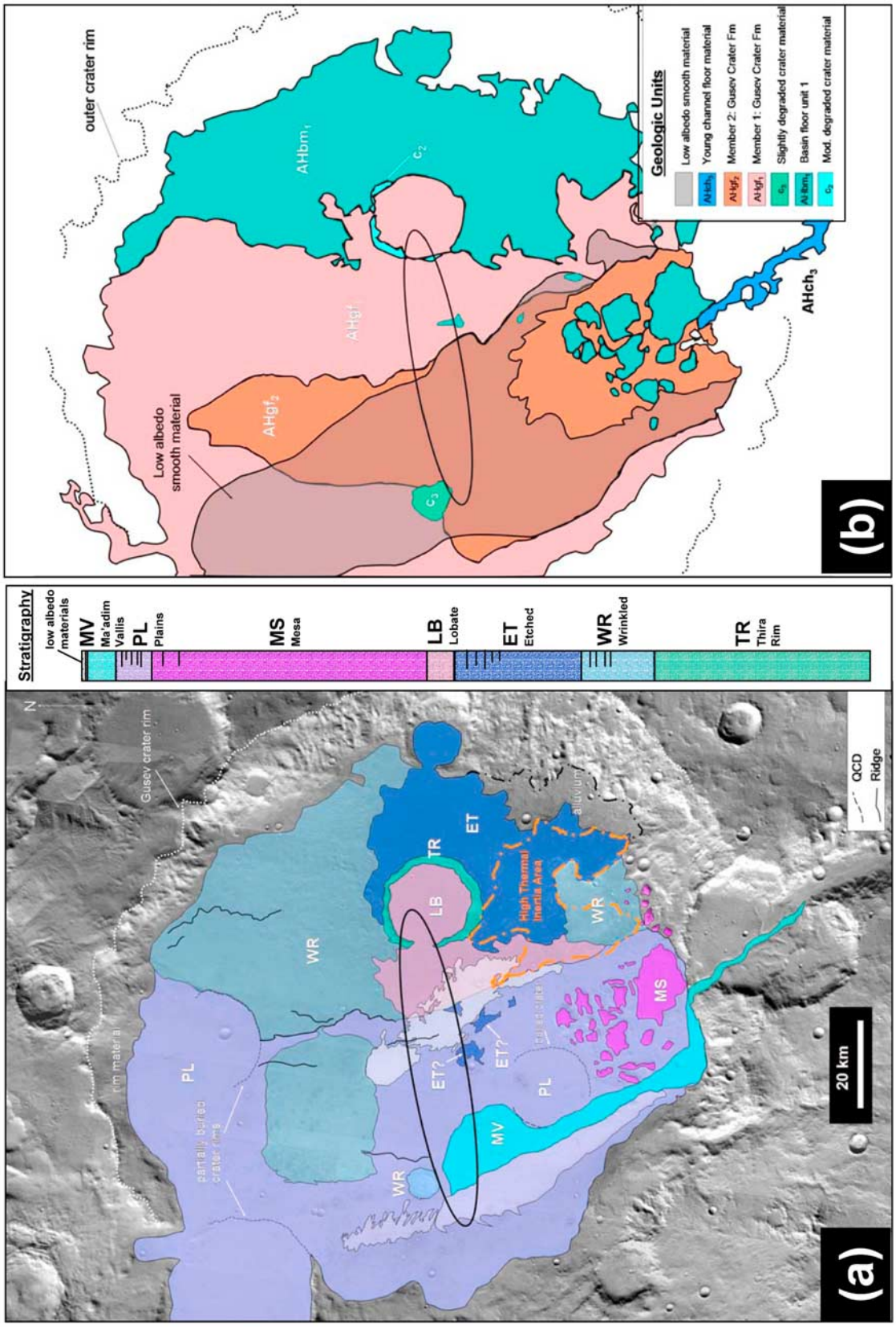

Figure 14. (a) Surface unit map of Gusev crater based on thermophysical, morphologic, topographic, and crater density data and (b) geologic map of Gusev crater from *Kuzmin et al.* [2000].

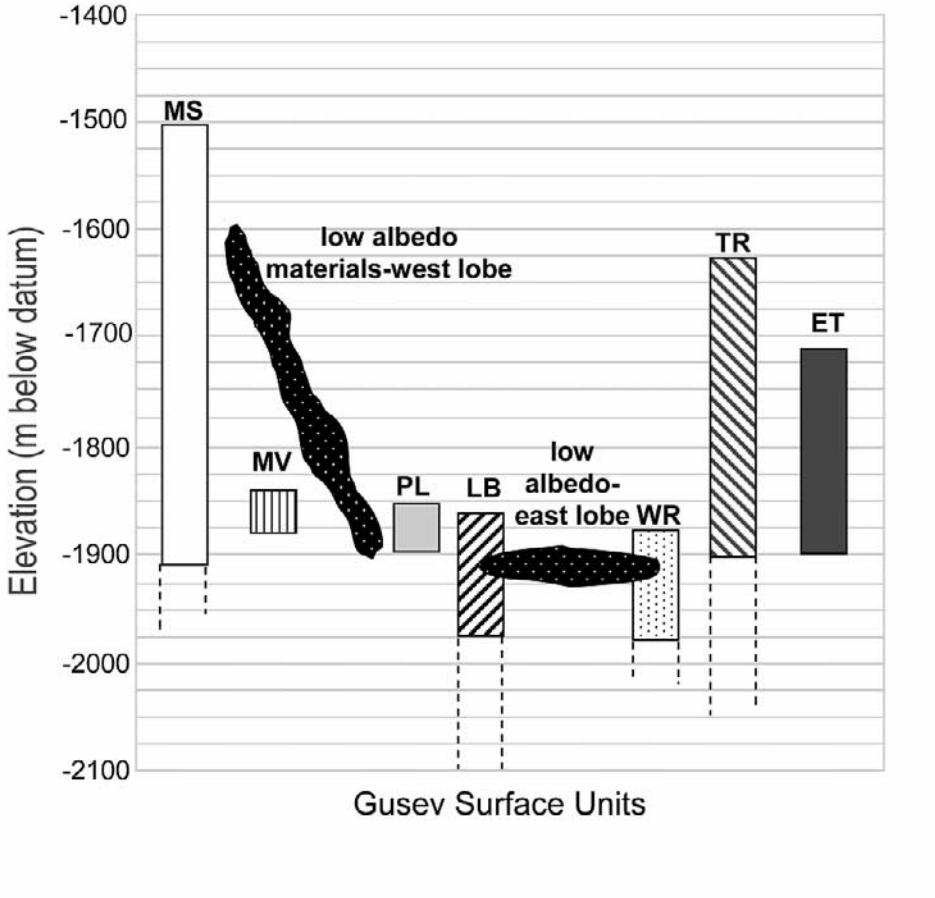

Figure 15. MOLA elevations of surface units within Gusev. Low-albedo materials are shown to illustrate their elevations and which units they overlie. The western low-albedo lobe overlies MV and PL, while the eastern lobe overlies LB and WR.

central Gusev (Figure 18). Here LB has been deposited against WR ridges and in the valleys in between. This confirms that WR was first deposited and later modified prior to LB deposition.

[48] While TR and WR have been demonstrated to be the oldest units within Gusev, the relationship between WR and other units is less clear. Crater density data suggests that WR deposition postdated that of ET. On the basis of the above discussion, an Early Amazonian age for WR is suspect. Although WR lies at lower elevations, its mean elevation is near −1905 m. When topographic profiles across ET-WR unit contacts in the north and southeast are considered (Figures 12a and 12b), a noticeable slope break at ∼−1900 m is observed. We propose this slope break as the topographic expression of WR underlying ET in southeastern Gusev.

[49] Conflicting age data also exist between WR and PL. Crater densities suggest a Late Noachian to Late Hesperian age for PL compared to the problematic Early Amazonian age for WR. Insight into the WR-PL relationship is provided by a broad ''window'' (topographic depression) in northwestern Gusev. This ''window'' shows some smaller ridges and degraded craters rims at the bottom of the depression that correspond to WR elevations. This suggests that WR under-

Table 2. Crater Density/Age Determination

		Crater Density (N > (x)km diam./10^6 km^2)[a]			
Unit Name	Unit Area, km^2	N(1)	N(2)	N(5)	Age Range[b]
PL	3230	2167	1238	310	UN-UH
WR	2945	111	185	0	LA-UA
ET	1249	1600	800	0	LH-UH
MS	439	2277	2277	0	UH
TR	∼163	0	0	0	
MV	549	3644	1822	0	LH
Low albedo	∼518	0	0	0	
LB	1152	3473	0	0	LH

[a]N, number of craters.
[b]UN, Upper Noachian; LH, Lower Hesperian; UH, Upper Hesperian; LA, Lower Amazonian; UA, Upper Amazonian.

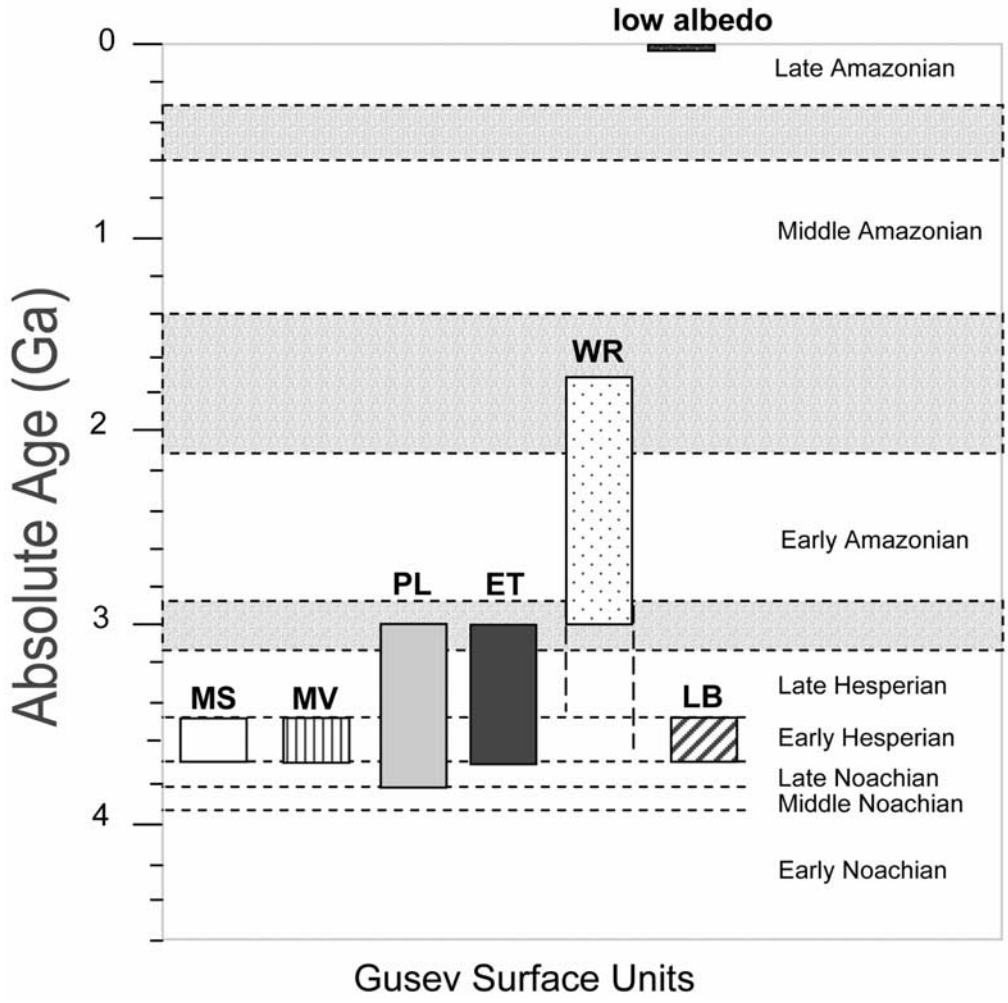

Figure 16. Age estimates for units based on crater density calculations. Bars represent the range in age estimates for 1, 2, and 5 km-diameter craters. Age boundaries for epochs are from *Tanaka* [1986].

lies PL, but could have resulted from erosion of PL and subsequent deposition of WR within basins. Comparison of the mean elevations for WR (−1905 m) and PL (−1865 m) supports the former hypothesis of WR underlying PL. This also suggests that PL may be relatively thin (<40 m). On the basis of this model, Crivitz crater, to the northwest of the landing ellipse, corresponds to WR elevations and has been mapped as WR (Figures 4b and 14a). LB overlies WR in central Gusev and PL occurs at higher elevations than LB, further supporting the proposed WR-PL age relationship. It is certain that PL is present in western Gusev, but its easternmost extent is unclear. An escarpment near the southeastern PL boundary and the lack of PL exposure in eastern Gusev implies that PL does not extend into the eastern half of Gusev. However, an indistinct slope break near −1874 m in the ET-WR escarpment of northeastern Gusev may represent the topographic expression of PL in this area, suggesting PL deposition in eastern Gusev prior to ET. Lack of PL deposition in eastern Gusev would imply that ET directly overlies WR. The overlap in Late Noachian and Late Hesperian ages between ET and PL could support coeval deposition. If ET and PL were syndepositional, then a facies change may exist between these units. In either case, deposition of ET is contemporaneous with or post-dates PL deposition.

[50] Although PL overlies LB and WR, the age relationship between PL and MS is less clear. Observations suggest that MS had been dissected. However, elevation data are not clear as to whether or not the PL depositional/erosional event was responsible. Crater densities (Figure 16) however, suggest a relatively younger age for PL indicating that PL deposition may post-date MS deposition. Because MV is at higher elevations than PL both within Ma'adim Vallis and Gusev, we propose that MV postdates PL. Crater densities show that MV deposition happened near the time of PL deposition.

[51] Finally, with the low-albedo material showing redistribution during previous Mars missions (Figure 11), it is clear that this material represents the last stratigraphic event in Gusev.

[52] Thira's calculated excavation depth (−3884 ± 413 m) does not extend to the initial estimated excavation depths of Gusev crater (−9326 ± 2848 m elevation respectively). Within minutes of most impact events (for complex craters), crater wall collapse sends target rock down toward the center of the transient crater, enlarging the crater diameter and infilling the transient cavity, reducing the crater depth. Gusev's initial modified crater depth is uncertain. The relationship of final crater depth, d, to final crater diameter,

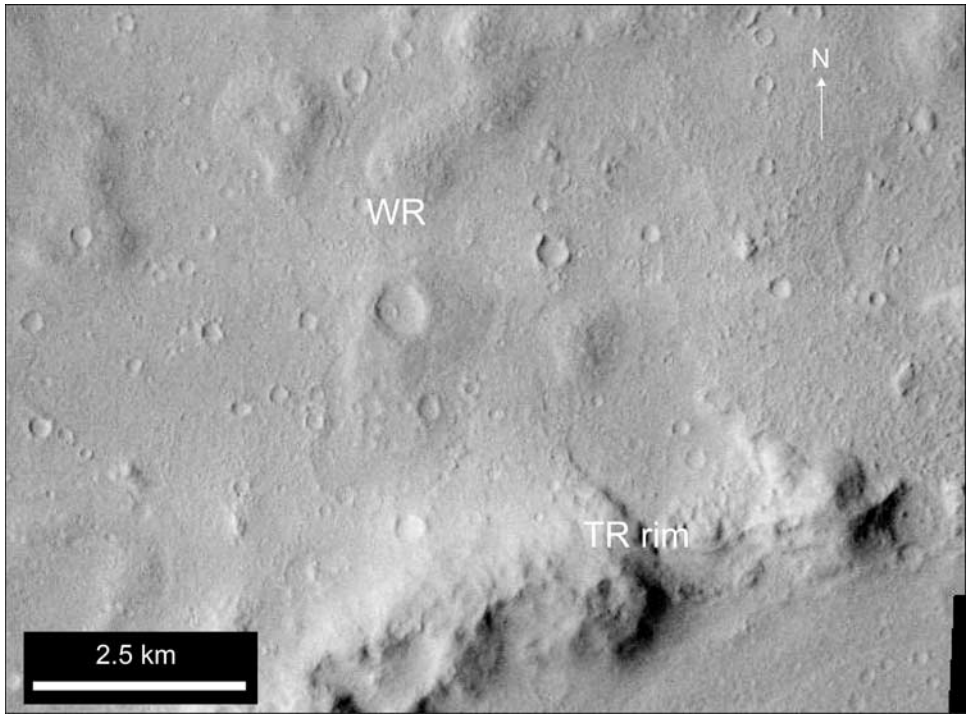

Figure 17. THEMIS Day TIR view of WR deposited against TR northwest of the crater rim (V01580003).

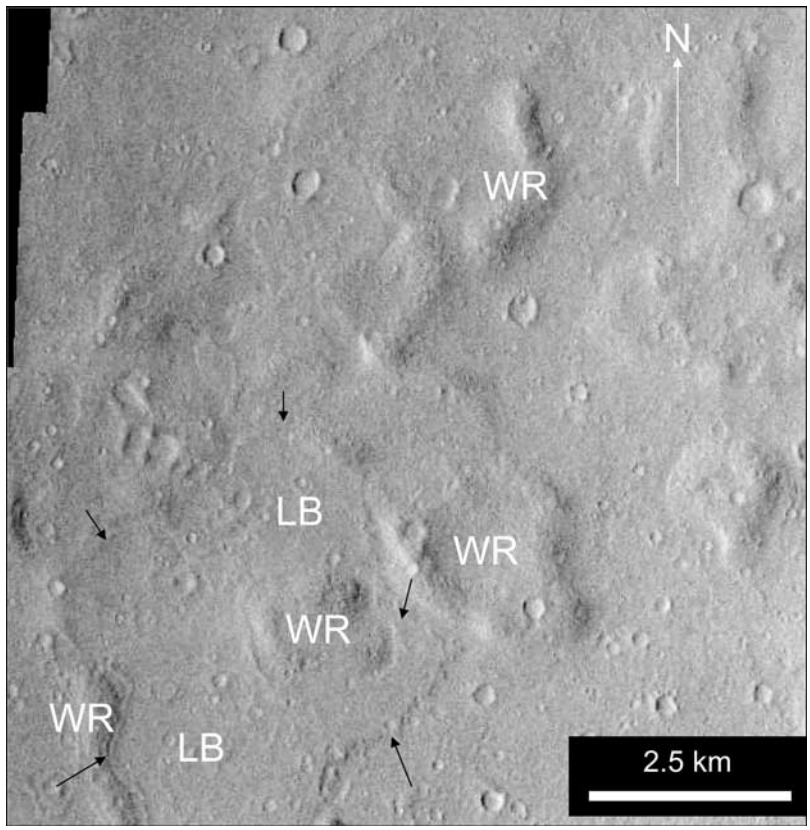

Figure 18. LB deposited against and between ridges of WR in north central Gusev (THEMIS-V-01580003).

D, for Martian craters (7 to 100 km diameter) was determined by *Smith et al.* [2001] to be $d = 0.33D^{0.53\pm0.03}$. This relationship was determined from measurements made by MOLA data of modified craters that are in various stages of exhumation and burial. If, for the moment, we assume that this morphometric relationship holds for the 150 km-diameter Gusev crater and that d represents the initial modified crater depth (between −4582 and −3092 m), then it is possible that Thira may have excavated slumped target rock material from an infilled Gusev. If this relationship does not hold for larger craters, it is still possible that Thira excavated basement material. Soon after the formation of complex craters, a central uplift forms (although Gusev shows no evidence of such a central peak). Thira crater, due to its proximity to Gusev's center, might have sampled basement in the central uplift. Such exhumation may have provided a means of sampling the oldest strata within Gusev.

[53] The stratigraphic column and surface unit map (Figure 14a) provide a basis for inferring the depositional/erosional history for units within Gusev crater. Following the Noachian impact event that formed Gusev [*Kuzmin et al.*, 1997, 2000], the Thira impact event exposed deep strata or basement. After Thira, WR was deposited (possibly across the entire floor of Gusev and perhaps preceded by deposition of older strata). Layering suggests multiple WR depositional episodes. Following WR deposition, ET was deposited and subsequently eroded. Lack of detection of ET beyond southeastern Gusev suggests that ET may represent localized deposition; however, exposed ~horizontal layering suggests that ET was laterally extensive and occurred in multiple episodes. The high degree of modification of the ET surface suggests extensive post-depositional erosion, with some areas resembling relict "channels" suggestive of fluid movement (Figure 10). LB deposition was concentrated in southwestern and central Gusev, as demonstrated by its terminal lobate margins (Figure 8d). This unit was deposited at some of the lowest crater elevations. PL deposition then followed in multiple depositional events. Subsequent MV deposition then represented the last depositional event related to Ma'adim Vallis. During the Early Amazonian, modification of the WR surface occurred. Long after this, low-albedo material was deposited and redistributed/re-exposed across Gusev.

4.5. Comparisons With Previous Work

[54] Analysis of THEMIS data, in context with TES, MOC, MOLA, and Viking Orbiter camera data sets has provided a new means of identifying local surface units on Mars and reconstructing their stratigraphic relationships and depositional/erosional histories. This approach can be compared to earlier studies [*Landheim et al.*, 1994; *Grin and Cabrol*, 1997b; *Kuzmin et al.*, 2000] that mapped surface units using Viking visible images and estimated elevations using photoclinometric and radar-based techniques. Newer Mars Odyssey and MGS instruments provide data related to thermophysical, morphological, topographic, crater density, and temporal relationships among units.

[55] The first geologic map of Gusev [*Landheim et al.*, 1994] identified six geologic units. This map was followed by the *Grin and Cabrol* [1997b] sedimentologic map, which included seven Gusev sedimentologic units. The USGS map [*Kuzmin et al.*, 2000] of Gusev (Figure 14b) was, like previous editions, based on analyses of Viking imagery and age calculations from crater density measurements. A distinction between our *surface unit* map and other "geologic" maps is that presently, no compositional data presently exists for surface units, which are necessary for use of the term *geologic unit*. Forthcoming analyses of THEMIS spectra may allow some compositional inferences to be drawn. Here we compare our surface unit map with that of *Kuzmin et al.* [2000].

[56] Although there is a rough correspondence between surface units from this study (Figure 14a) and the previously mapped "geologic" units of *Kuzmin et al.* [2000] (Figure 14b), some differences are apparent. TR corresponds to a distinct geologic unit of Moderately Degraded Crater Material (c_2). ET, in southeastern Gusev, corresponds to the southern half of Basin Floor Unit 1 $AHbm_1$, whereas WR correlates with both Gusev Crater Formation Member 1 $AHgf_1$ and $AHbm_1$. One of several WR outliers near the middle of the landing site ellipse was recognized as $AHbm_1$ on the geologic map. LB corresponds to $AHgf_1$. PL corresponds mostly with Gusev Crater Formation Member 2 ($AHgf_2$). MS mesas are distinctive in their thermophysical and morphological properties and thus are assigned to a distinct surface unit, but were correlated with $AHbm_1$ on the geologic map. MV is equivalent to Young Channel Floor Material ($AHch_3$) within Ma'adim Vallis, but with the extension of MV basinward, MV is shown to correlate with $AHgf_2$ and Low Albedo Smooth Material as well. The two parallel bands of low-albedo material now covering parts of $AHgf_1$ and $AHgf_2$ were represented by a larger band of low-albedo smooth material in previous geologic mapping (derived from Viking imagery), demonstrating temporal changes in the distribution of these units.

[57] Several different stratigraphic sequences have been proposed for Gusev [*Landheim et al.*, 1994; *Cabrol et al.*, 1998; *Kuzmin et al.*, 2000]. The various stratigraphic models are compared with ours in Figure 19. Comparisons are complicated by different unit definitions. In comparing our stratigraphic column to that of *Kuzmin et al.* [2000], there is general agreement in the overall depositional sequence, with the exception of the timing of ET, LB, and MS depositional events. *Kuzmin et al.* [2000] considered ET, WR, and MS as a single unit, $AHbm_1$. Our model also correlates well with the depositional sequence of *Landheim et al.* [1994], with the exception of low-albedo material deposition (or exhumation). The *Cabrol et al.* [1998] model considers units outside of Gusev and does not subdivide the floor of Gusev into separate units.

4.6. Depositional Models

[58] Was Gusev truly a fluvio-lacustrine depocenter for much of Martian history, as interpreted by others [*Schneeberger*, 1989; *Cabrol et al.*, 1993, 1998; *Grin et al.*, 1994; *Grin and Cabrol*, 1997b]? Could volcanic or aeolian deposition be plausible depositional models for Gusev, or could all of these have contributed? Here we consider three hypotheses for unit deposition within Gusev crater: (1) sedimentary, (2) volcanoclastic, or (3) volcanoclastic-sedimentary.

[59] The first model involves deposition of strata entirely by sedimentary processes, either in fluvial and/or lacustrine settings as proposed by others [*Schneeberger*, 1989; *Cabrol et al.*, 1993, 1998; *Grin et al.*, 1994; *Grin and Cabrol*,

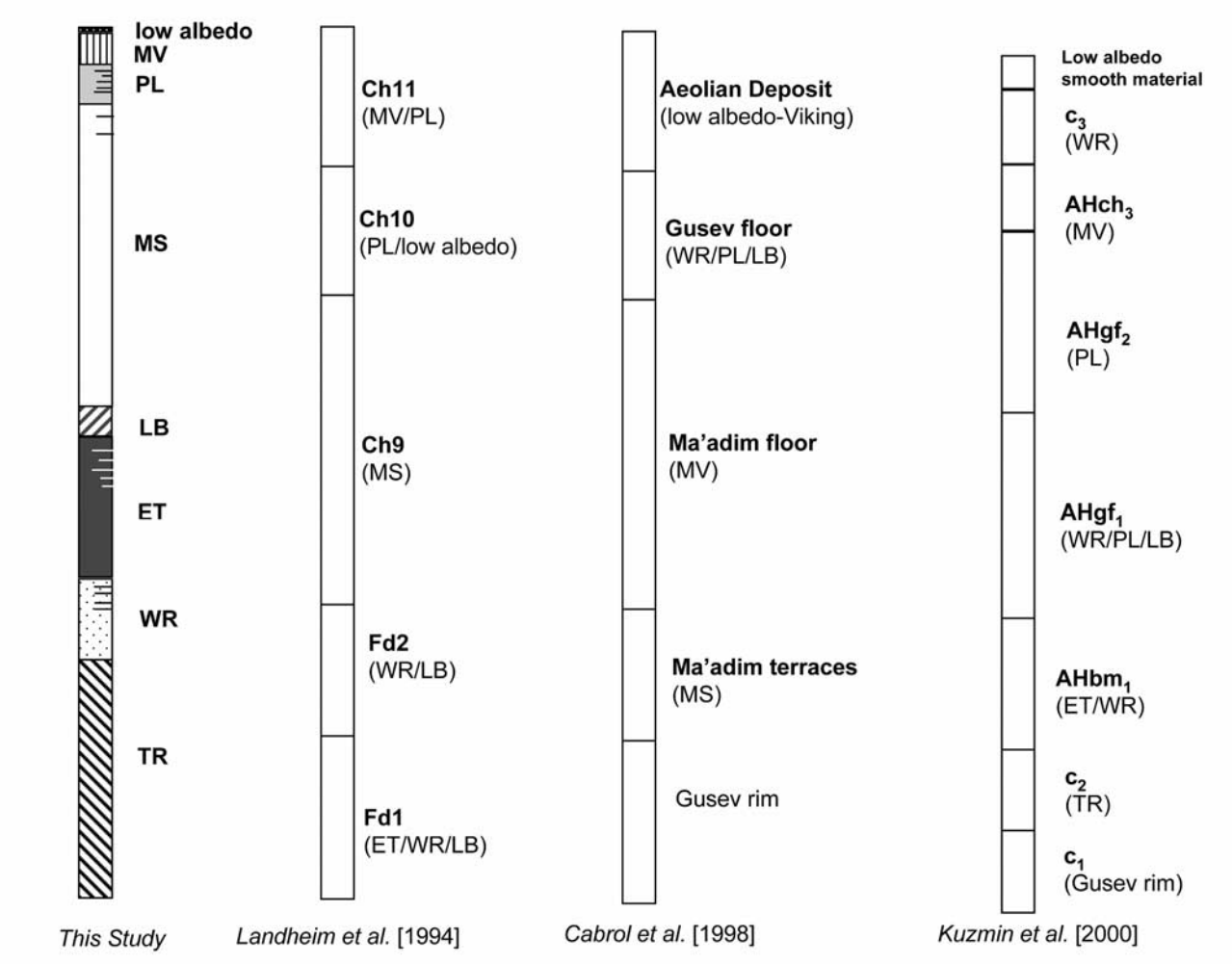

Figure 19. Comparisons of the *Landheim et al.* [1994], *Cabrol et al.* [1998], and *Kuzmin et al.* [2000] stratigraphic models to that proposed in this study.

1997b]. Surface units within Gusev appear as horizontal to sub-horizontal units that show basin-wide or localized deposition. Original horizontality, while not unique to sedimentary regimes, does appear to occur within Gusev and may suggest sedimentary deposition. While horizontal units in Gusev may represent deposition under a lacustrine regime, present data sets (MOC and THEMIS) do not provide the resolution needed to identify uniquely lacustrine features.

[60] Under a fluvio-lacustrine regime, changing lacustrine base levels could account for varying geographic extents of geologic units. Initially, deposition of the basin-wide WR would represent normal, quiet water deposition of silt and clay across the basin. A rising base level would have then led to deposition of ET across Gusev, filling it to levels of at least −1710 m below datum. Base level in Gusev would then have dropped and LB would have been subaerially deposited within western and central Gusev. *Cabrol* [2002] interpreted LB's lobate margins as terraced shorelines. The morphology and changing elevations over which LB is deposited do not agree with this. Rather, it appears that the lobate margins represent the termination of flow against ET (in the southeast) and WR (in central Gusev). The morphology of this unit is possibly consistent with deposition by sub-lacustrine turbidity currents. The lobate nature of LB's terminal margins is more consistent with deposition by debris flow or as a "slurry" of material. Though the relative timing of PL and MS deposition is unclear, crater ages and the dissected nature of MS suggest that MS was deposited prior to PL. A rising base level (to at least −1500 m) would then account for the later deposition of MS at the terminus of Ma'adim. The sudden change from the higher-energy regime of Ma'adim to the lower-energy regime of standing water in Gusev would result in dumping of sediment as "deltaic" deposits at the interface. In terrestrial deltas, deposition of sediment along slopes results in foreset bedding. Weakly exposed layering in MS appears to be horizontal, with a lack of dipping strata, suggesting that MS may not be deltaic in origin. An alternative to this could be that MS was a basin-wide deposit, subsequently eroded away from most of Gusev. Depending upon the true lateral extent of PL, deposition may have been more localized (suggestive of fluvial settings) or basin-wide (suggesting a somewhat higher base levels between −1865 and −1905 m). Either scenario would represent a reduced base level from the time of MS deposition. Subsequent, localized deposition of MV would have resulted from even lower base levels under a fluvial setting. A fluvio-lacustrine

regime could account for the changing morphology of MV from Ma'adim to Gusev. The linear ridges parallel to the long axis of Ma'adim Vallis continue until the breach in Gusev's southern rim. Once inside Gusev, the characteristic MV texture is lost. This could indicate constrained valley flow toward the crater rapidly changing into flow across the broader plain of the crater floor. Another moderate rise in base level could account for sub-lacustrine modification of WR during the Early Amazonian. Eventual evacuation of water from Gusev would have led to the present-day aeolian regime. Under this model, fluvio-lacustrine activity would have dominated during the Hesperian, suggesting a period of hydrologic activity of <1 Ga, as opposed the <2 Ga period proposed by *Grin and Cabrol* [1997b] and *Cabrol et al.* [1998]. However, standing lake levels as late as the Early Amazonian may have occurred, modifying WR, extending this period to <2 Ga.

[61] Thermal inertia values for surface units, under a fluvio-lacustrine regime, should be expected to correlate with values expected from sediment or sedimentary rock. Interpretations of surfaces covered by $\leq$ sand-sized particles for two surface units (PL and WR) and low-albedo material are consistent with this. However, these thermal inertias are from the uppermost regolith and may not be representative of the entire surface unit. Also, under this model, thermal inertias of units (such as MV or PL) extending from Ma'adim into Gusev should consistently change as depositional energies (and thus particle size distribution) change. This trend is not readily observable in TES data, but may be masked by dust covering surface units.

[62] Our consideration of the fluvio-lacustrine hypothesis does not preclude the role of aeolian deposition within Gusev. Aeolian erosion and deposition are the only processes that presently occur. Wind streaks, dust-devil tracks, and small dune fields have been observed superimposed on surface units, indicating more recent activity. We have not yet observed "fossil" aeolian bedforms within surface units or their layers; however, current data sets lack the resolution to identify and distinguish between "fossil" aeolian and fluvio-lacustrine sedimentary structures.

[63] A volcanoclastic model may also account for the distribution and orientation of some units and layering within Gusev. Horizontal layering occurs in many terrestrial and Martian lava flows and ash deposits. Apollinaris Patera, to the northeast, would be a candidate source area for such material. Surface types 1 and 2, thought to represent volcanic lithologies [*Bandfield et al.*, 2000; *Hamilton et al.*, 2001; *Wyatt and McSween*, 2002], have been detected in low-albedo material in Gusev; however, visible imagery and TES thermal inertia data suggest that these are likely aeolian sand. Observations of the northwestern rim of Gusev (Figure 1a) suggest that Apollinaris lava flows did not extend as far as Gusev. Nevertheless, explosive volcanic episodes during the Hesperian may have deposited ash within Gusev [*Robinson et al.*, 1993]. Surface unit ages do correspond to the timing of Apollinaris volcanic activity. Prevailing winds at the time of eruption could have carried ash fall southeastward toward Gusev. Under this model, variability in layering weathering profiles could be explained by ash compositional variability or the degree of induration of ash falls. However, comparisons of slope angles for Apollinaris Patera with other Martian phreatomagmatic and shield volcanoes, suggest less-energetic explosive activity and thus fewer distal fall deposits [*Thornhill et al.*, 1993]. This model alone cannot account for the localized deposition of units such as LB, MS, MV, and potentially ET and PL, but may account for deposition of WR and the low-albedo material. Because this model considers Apollinaris Patera the most likely volcanic source area, volcanoclastic deposits would thus thicken northwestward across Gusev. Presently, there is no indication that such thickening occurs. If such thickening once existed, it may have been subsequently modified by erosional processes.

[64] Because neither of the above models provides a unique solution for deposition within Gusev, a combined volcanoclastic-sedimentary model is considered. This model proposes syndepositional and/or alternating volcano-sedimentary deposits within Gusev. It evokes fluvial and/or aeolian processes for localized deposition, while lacustrine and ash-fall activity could account for basin-wide deposition. Pronounced weathering profiles could also be explained by changes in rock type or other factors mentioned above.

[65] With the limitations placed on the volcanoclastic model, it is the least favored of the three. The volcanoclastic-sedimentary model is the most preferred because it accounts for both localized and widespread deposition within Gusev and recognizes the potential influx of ash-fall deposits from nearby Apollinaris Patera. Even if explosive activity were less energetic, leading to lower plume heights, prevailing wind patterns could serve to transport ash over 350 km to Gusev crater. With such minimal activity and long transport distances, the role of volcanic deposition is diminished as compared to sedimentary processes. While the results of our study are consistent with Gusev as a fluvio-lacustrine depocenter, we have yet not identified features that are uniquely lacustrine.

4.7. MER Testable Hypotheses

[66] Regardless of the exact depositional/erosional history of Gusev crater, this study has demonstrated the geologic variability of the site (five or more of the seven surface units mapped in this study lie within the MER-A landing ellipse). With such heterogeneity, the possibility of sampling materials transported from proximal units (by aeolian, fluvial, or impact processes) during MER rover traverses (<1 km) is high relative to other candidate landing sites.

[67] A MER rover in Gusev would provide an opportunity to calibrate remote-sensing data collected by the orbiting THEMIS and TES instruments. Mini-TES will have the ability to measure albedo, thermal inertia, and temperature, as well as the capability of collecting spectra from dust-free surfaces, which could be used to compare surface compositions derived from the THEMIS and TES instruments. The ability to "ground-truth" remote-sensing data may lead to more accurate interpretations of Gusev geology.

[68] Instruments on MER provide a means of testing depositional models and determining stratigraphic relationships of units within Gusev. Spectral analyses from Mini-TES and APXS may provide data with which to identify rock types and thus clarify depositional regimes. Pancam and Microscopic Imager could reveal textures within strata indicative of depositional parameters (i.e., energy of environment). Pancam, APXS, and Mini-TES could discriminate rock types, thus noting contributions from various deposi-

tional sources (fluvio-lacustrine, aeolian, volcanoclastic). In addition, imaging instruments may be used to determine the true nature of some unit contacts (i.e., stratigraphic position, conformable vs. non-conformable) within Gusev.

[69] MER traverses will occur within only a limited portion (<1 km) of the MER-A landing ellipse. Considering this, we take a closer look at the geology of the landing ellipse (Figure 14a) from east to west, examining previous hypotheses and how MER might test them.

[70] A landing near the rim of Thira crater provides an opportunity to examine the TR and LB units. Is TR different spectrally (and thus compositionally) from LB, or did the Thira impact event sample a lower portion of WR? Analyses of rim material may also determine whether dark patches along the Thira rim is aeolian drifts of low-albedo material or exposed bedrock.

[71] Traverses farther west would likely encounter exposures of LB, PL, and low-albedo material. Analyses of low-albedo material in this area may indicate whether or not it overlies PL and LB or simply represents a scouring of the PL and LB surfaces. A landing on the eastern side of the escarpment between LB and PL/low-albedo material exposures could provide an opportunity to examine further the stratigraphic relationships and note the presence of additional strata not measured in this study.

[72] The center of the landing ellipse is dominated by the PL unit, which, if determined to represent fluvial deposition, provides a means of analyzing sediment from Ma'adim source regions [*Irwin et al.*, 2002]. Although PL is the dominant unit here, there are several craters that likely sampled subsurface strata (below the inferred 40 m thickness for PL). The measured depth (>1900 m) of an unnamed crater (Figure 13d) indicates that it likely excavated LB and WR strata, providing a means for MER to sample these strata. Elevation measurements from another crater northwest of the landing ellipse (Figure 13b) also indicate that this impact event sampled WR, ejecting material into the landing ellipse.

[73] Two isolated areas within the landing ellipse (Figure 14a; labeled as ET_t?) may provide access to other units. Each exposes material that morphologically, has an "etched" appearance, suggestive of ET. They also have nighttime TIR temperatures comparable to western ET. In daytime TIR, each window has thermophysical properties consistent with LB, ET, or the material immediately underlying PL. MOLA data show elevations consistent with PL and ET. MER traverses in this area may allow for the distinction between PL and ET for these areas. The presence of ET within the landing ellipse would further add to the geologic diversity of the ellipse.

[74] Quasi-Circular Depressions (QCDs), first identified on Mars by *Frey et al.* [1999], may also provide a means of sampling from Gusev's sub-surface strata within the landing ellipse. A Quasi-Circular Depression (QCD) within the southwestern portion of the landing ellipse has been detected (at 14.96°S, 175.04°E) from MOLA data (Figure 4b). This QCD, first identified by *Kuzmin et al.* [2000], is thought to represent a buried crater. Its rim has yet to be noted in visible or TIR data; however, a circular positive relief feature (−1820 to −1860 m) has been detected using MOLA data and is thought to represent the surficial expression of the crater rim. Measured rim diameters and heights have allowed us to calculate the transient crater diameter [*Croft*, 1985] and excavation depth for this QCD. This crater would have penetrated to depths of −3300 to −4000 m, well below the lowest exposed WR. Like Thira crater, this QCD may have sampled WR strata or older units. A landing near the center of the ellipse thus provides MER a means of sampling subsurface stratigraphy to address the following questions: (1) What are the stratigraphic relationships between PL, LB, WR, and potentially older units? (2) Are these units spectrally (and perhaps compositionally) distinct from each other? (3) Has Gusev's depositional environment changed from its early history?

[75] MER traverses within the western portion of the landing ellipse would also permit the examination of low-albedo material and PL, but more importantly, could allow the nature of MV to be determined. Is MV a real surface unit within Gusev, or does it represent a thermophysically distinct area within the PL unit? If it is a distinctive surface unit, how does it compare spectrally with PL? Does it represent a final stage of fluvial deposition? Answers to these questions would provide insight into Gusev's late-stage depositional environments.

[76] It is clear that the MER-A landing ellipse lies within a geologically heterogeneous area of Mars and of Gusev itself. If this heterogeneity represents changes in a single or multiple depositional environments, then direct analyses of Gusev surface units by MER may provide insight into changing geologic/climatic conditions over a significant interval of Martian geologic history. More importantly, MER would provide a means of examining the geologic and climatic record of Mars over an extended and important (Noachian-Hesperian) interval of Martian history.

5. Summary

[77] Gusev crater is a candidate site for MER because of its suspected former fluvio-lacustrine environment. This study has used high spatial-resolution data from THEMIS, supplemented by TES, MOC, and MOLA data, to identify units comprising the floor of Gusev and Ma'adim Vallis. Thermophysical and morphologic unit maps show broad correlations, supporting the validity of the seven proposed surface units, as follows:

[78] ● Ma'adim Vallis (MV) – THEMIS nighttime cold material (occurring as parallel ridges in the valley) from Ma'adim Vallis appearing to extend into Gusev

[79] ● Plains (PL) – unit trending from Ma'adim to northwest breach in Gusev's rim with hot nighttime TIR craters

[80] ● Mesa (MS) – dissected mesas with cold nighttime tops and hot TIR slopes

[81] ● Lobed (LB) – flat, freshly-cratered surface with distinctive lobate margins

[82] ● Etched (ET) – unit with a "mottled" daytime/nighttime TIR appearance and apparently eroded surface

[83] ● Wrinkled (WR) – unit with low, north-south oriented ridges that contains cold nighttime TIR craters

[84] ● Thira Rim (TR) – unit exposed along Thira crater rim; hot nighttime TIR material; strata exhumed from depth.

[85] ● Also observed were low-albedo materials that have apparently been redistributed/reexposed by aeolian processes since the Viking program.

[86] Observations of the surface unit map and MOLA topography data allowed us to define Gusev's stratigraphy and thus infer a depositional/erosional history for the crater interior. The stratigraphic order (top to bottom), is as presented above. The existence of seven surface units, and layering within these units, suggests multiple depositional and erosional events. Observations are consistent with deposition by fluvial, lacustrine, volcanoclastic, and/or aeolian processes. Landing a MER rover in Gusev would probably allow sampling of multiple surface units, would provide ground truth for orbital remote-sensing measurements, and would test a number of hypotheses about surface and geologic units in the interior of Gusev offered in this and previous papers.

[87] **Acknowledgments.** This work was partly supported by NASA subcontract 01-082 from Arizona State University (HYM), JPL-1241129 (JEM), and the 2001 Mars Odyssey Science Office (PRC). Thanks also to Victoria Hamilton, Stephan van Gasselt, Ken Edgett, Melissa Lane, and Jim Rice for their insightful reviews of our work.

References

Bandfield, J. L., V. E. Hamilton, and P. R. Christensen, A global view of Martian surface compositions from MGS-TES, *Science*, *287*(5458), 1626–1630, 2000.

Cabrol, N. A., Gusev crater (MER A): Overview of relevance, science, and testable hypotheses, paper presented at Mars Exploration Rover Landing Site Workshop, Pasadena, Calif., 26–28 March 2002.

Cabrol, N. A., and A. Brack, Episodic oasis for water-dependent life on Mars, *Proc. Lunar Planet. Sci. Conf. 26th*, 201–202, 1995.

Cabrol, N. A., and E. A. Grin, Hydrogeology and exobiology significance of Martian large crater lakes, in *Conference on Early Mars: Geologic and Hydrologic Evolution*, *Physical and Chemical Environments*, *and the Implications for Life*, edited by S. M. Clifford et al., pp. 14–15, Lunar and Planet. Inst., Houston, Tex., 1997.

Cabrol, N. A., E. A. Grin, A. Dollfus, and G. Dawidowicz, An ancient inner lake in Ma'adim Vallis, *Proc. Lunar Planet. Sci. Conf. 24th*, 241–242, 1993.

Cabrol, N. A., R. Landheim, R. Greeley, and J. D. Farmer, Fluvial processes in Ma'adim Vallis and the potential of Gusev crater as a high priority site, *Proc. Lunar Planet. Sci. Conf. 25th*, 213–214, 1994.

Cabrol, N. A., E. A. Grin, V. C. Gulick, C. P. McKay, R. Greeley, M. Sims, and G. Briggs, Rover mobility and sampling strategy on Mars: The case for Gusev crater, *Proc. Lunar Planet. Sci. Conf. 26th*, 189–190, 1996.

Cabrol, N. A., R. Landheim, and E. A. Grin, Ma'adim Vallis paleocourses, *Proc. Lunar Planet. Sci. Conf. 28th*, 195–196, 1997.

Cabrol, N. A., E. A. Grin, R. Landheim, R. O. Kuzmin, and R. Greeley, Duration of the Ma'adim Vallis/Gusev crater hydrogeologic system, Mars, *Icarus*, *133*, 98–108, 1998.

Cabrol, N. A., E. A. Grin, and D. Fike, Gusev Crater: A landing site for MER, *Lunar Planet. Sci.* [CD-ROM], *XXXIII*, abstract 1142, 2002.

Christensen, P. R., D. L. Anderson, S. C. Chase, R. N. Clark, H. H. Kieffer, M. C. Malin, J. C. Pearl, and J. Carpenter, Thermal emission spectrometer experiment; Mars Observer mission, *J. Geophys. Res.*, *97*(5), 7719–7734, 1992.

Christensen, P. R., et al., Mars Global Surveyor Thermal Emission Spectrometer experiment: Investigation description and surface science results, *J. Geophys. Res.*, *106*(E10), 23,823–23,871, 2001.

Christensen, P. R., et al., Morphology and composition of the surface of Mars: Mars Odyssey THEMIS results, *Science*, *300*, 2056–2061, 2003.

Crater Analysis Technique Working Group, Standard techniques for presentation and analysis of crater-size frequency data, *Icarus*, *37*(2), 467–474, 1979.

Croft, S. K., The scaling of complex craters, *Proc. Lunar Planet. Sci. Conf. 15th*, Part 2, *J. Geophys. Res.*, *90*, suppl., C828–C842, 1985.

Edgett, K. S., and M. C. Malin, The layered upper crust of Mars: An update on MGS MOC observations after two years in the mapping orbit, *Lunar Planet. Sci.* [CD-ROM], *XXXIV*, abstract 1124, 2003.

Eugster, H. P., and L. A. Hardie, Saline lakes, in *Lakes: Chemistry, Geology, Physics*, edited by A. Lernam, pp. 237–293, Springer-Verlag, New York, 1978.

Farmer, J. D., and D. Des Marais, Exploring for a record of ancient Martian life, *J. Geophys. Res.*, *104*(E11), 26,977–26,995, 1999.

Frey, H., S. E. H. Sakimoto, and J. H. Roark, Discovery of a 450 km diameter, multi-ring basin on Mars through analysis of MOLA topographic data, *Geophys. Res. Lett.*, *26*(12), 1657–1660, 1999.

Grin, E. A., and N. A. Cabrol, Antarctic analog for a perennial ice-covered paleolake in Gusev Crater (Mars), *Proc. Lunar Planet. Sci. Conf. 28th*, 473–474, 1997a.

Grin, E. A., and N. A. Cabrol, Limnologic analysis of Gusev crater paleolake, Mars, *Icarus*, *130*, 461–474, 1997b.

Grin, E. A., and N. A. Cabrol, Subglacial rotary currents in Gusev Crater paleolake (Mars), *Proc. Lunar Planet. Sci. Conf. 28th*, 475–476, 1997c.

Grin, E. A., N. A. Cabrol, and G. Dawidowicz, Proposal for a topographic survey of Gusev Crater, *Lunar Planet. Sci.*, *XXV*, 483–484, 1994.

Hamilton, V. E., M. B. Wyatt, H. Y. McSween Jr., and P. R. Christensen, Analysis of terrestrial and Martian volcanic compositions using thermal emission spectroscopy: 2. Application to Martian surface spectra from the Mars Global Surveyor Thermal Emission Spectrometer, *J. Geophys. Res.*, *106*(E7), 14,733–14,746, 2001.

Irwin, R. P., III, T. A. Maxwell, A. D. Howard, R. A. Craddock, and D. W. Leverington, A large paleolake basin at the head of Ma'adim Vallis, *Mars, Science*, *296*, 2209–2212, 2002.

Jakosky, B. M., and M. T. Mellon, High-resolution thermal inertia mapping of Mars: Sites of exobiological interest, *J. Geophys. Res.*, *106*(E10), 23,887–23,907, 2001.

Kuzmin, R. O., R. Greeley, R. Landheim, and N. A. Cabrol, Geologic mapping of Gusev crater-Ma'adim Vallis region, Mars, *Lunar Planet. Sci.*, *XXVIII*, 779–780, 1997.

Kuzmin, R. O., R. Greeley, R. Landheim, N. A. Cabrol, and J. D. Farmer, Geologic map of the MTM-15182 and MTM-15187 quadrangles, Gusev Crater-Ma'adim Vallis Region, Mars, in *Geologic Investigative Series*, 8 pp., 1 sheet, U.S. Geol. Surv., Reston, Va., 2000.

Landheim, R., R. Greeley, D. Des Marais, J. D. Farmer, and H. Klein, Mars exobiology landing sites for future exploration, *Proc. Lunar Planet. Sci. Conf. 24th*, 845–846, 1993.

Landheim, R., N. A. Cabrol, R. Greeley, and J. D. Farmer, Strategic assessment of Gusev crater as an exobiology landing site, *Proc. Lunar Planet. Sci. Conf. 25th*, 769–770, 1994.

Malin, M. C., and K. S. Edgett, Mars Global Surveyor Mars Orbiter Camera: Interplanetary cruise through primary mission, *J. Geophys. Res.*, *106*(E10), 23,429–23,570, 2001.

Malin, M. C., G. E. Danielson, A. P. Ingersoll, H. Masursky, J. Veverka, M. A. Ravine, and T. A. Soulanille, Mars Observer Camera, *J. Geophys. Res.*, *97*, 7699–7718, 1992.

Masursky, H., A. L. J. Dial, M. E. Strobell, and D. J. Applebee, Recent progress in the study of MRSR (Mars Rover Sample Return) candidate landing sites, *Proc. Lunar Planet. Sci. Conf. 19th*, 730–731, 1988.

Pelkey, S. M., B. M. Jakosky, and M. T. Mellon, Thermal inertia of crater-related wind streaks on Mars, *J. Geophys. Res.*, *106*(E10), 23,909–23,920, 2001.

Pierazzo, E., and H. J. Melosh, Understanding oblique impacts from experiments, observations, and modeling, *Annu. Rev. Earth Planet. Sci.*, *28*, 141–167, 2000.

Robinson, M. S., P. J. Mouginis-Mark, J. Zimbleman, and S. S. C. Wu, Chronology, eruption duration and atmospheric contribution of Apollinaris Patera, Mars, *Proc. Lunar Planet. Sci. Conf. 24th*, 1209–1210, 1993.

Schneeberger, D. M., Episodic channel activity at Ma'adim Vallis, Mars, *Proc. Lunar Planet. Sci. Conf. 20th*, 964–965, 1989.

Smith, D. E., et al., Mars Orbiter Laser Altimeter: Experimental summary after the first year of global mapping of Mars, *J. Geophys. Res.*, *106*(E10), 23,689–23,722, 2001.

Squyres, S. W., et al., Athena Mars Rover science investigation, *J. Geophys. Res.*, *108*(E12), 8062, doi:10.1029/2003JE002121, in press, 2003.

Tanaka, K. L., The stratigraphy of Mars, *Proc. Lunar Planet. Sci. Conf. 17th*, Part 1, *J. Geophys. Res.*, *91*, suppl., E139–E158, 1986.

Thornhill, G. D., D. A. Rothery, J. B. Murray, A. C. Cook, T. Day, J. P. Muller, and J. C. Iliffe, Topography of Apollinaris Patera and Ma'adim Vallis: Automated extraction of digital elevation models, *J. Geophys. Res.*, *98*(E12), 23,581–23,587, 1993.

Wyatt, M. B., and H. Y. J. McSween, Spectral evidence for weathered basalt as an alternative to andesite in the northern lowlands of Mars, *Nature*, *417*(6886), 263–266, 2002.

Zuber, M. T., D. E. Smith, S. C. Solomon, D. O. Muhleman, J. W. Head, J. B. Garvin, J. B. Ashire, and J. L. Bufton, The Mars Observer Laser Altimeter investigation, *J. Geophys. Res.*, *97*, 7781–7797, 1992.

P. R. Christensen and M. B. Wyatt, Department of Geological Sciences, Arizona State University, Tempe, AZ, USA.

A. Ghosh, H. Y. McSween Jr., K. A. Milam, J. E. Moersch, K. R. Stockstill, and L. L. Tornabene, Planetary Geosciences Institute, Department of Geological Sciences, University of Tennessee, 306 Geological Sciences Building, Knoxville, TN 37996-1410, USA. (kmilam@utk.edu)